CYCLOIDEA paralogs function redundantly to specify dorsal flower development in *Mimulus lewisii* (Phrymaceae)

By

Taryn Sena Dunivant
B.Sc., University of California, Santa Cruz, 2017

Submitted to the graduate degree program in Ecology and Evolutionary Biology and the Graduate Faculty of the University of Kansas in partial fulfillment of the requirements for the degree of Master of Arts.

Chair: Dr. Lena Hileman

Dr. John Kelly

Dr. Jamie Walters

Date Defended: 27 August 2021

The thesis committee for Taryn Sena Dunivant certifies that this is the approved version of the following thesis:

CYCLOIDEA paralogs function redundantly to specify dorsal flower development in *Mimulus lewisii* (Phrymaceae)

Chair: Dr. Lena Hileman

Date Approved: 31 August 2021

Abstract

Repeated independent transitions between radial and bilateral flower symmetry have occurred across the angiosperm phylogeny, contributing to the vast diversity we see in floral morphology. The genetic program for bilateral flower symmetry has been documented in the model system *Antirrhinum majus* where the paralogs *CYCLOIDEA* (*CYC*) and *DICHOTOMA* (*DICH*) have partially redundant functions in establishing dorsal petal identity. These paralogs resulted from a duplication event in the ECE-*CYC2* gene lineage. Within Lamiales, at least 12 additional duplications in the ECE-*CYC2* lineage have occurred. The close homologs *CYC1* and *CYC2* resulted from one of these additional duplication events at the base of the higher core Lamiales (HCL).

In this study, we are using the emerging model *Mimulus lewisii* (Phrymaceae, HCL), to test for conservation of *MlCYC1* and *MlCYC2* in flower symmetry development, and whether these genes similarly function redundantly compared to *AmCYC* and *AmDICH*. Using *Agrobacterium*-mediated stable transformation techniques and RNA interference (RNAi), we were able to characterize *MlCYC1* and *MlCYC2* RNAi silenced lines. In addition, by cross-pollinating *MlCYC1* and *MlCYC2* single lines, we generated and characterized double *MlCYC1:MlCYC2* RNAi silenced lines. Our results from RNAi silencing, and consistent with our gene expression analyses, demonstrate that *MlCYC1* and *MlCYC2* together function to specify dorsal flower identity. Additionally, we find extensive functional redundancy between the paralogs *MlCYC1* and *MlCYC2*, with *MlCYC1* playing the dominant role in establishing dorsal petal identity. These results are consistent with what is found in *A. majus*, nonetheless the paralogs arose from independent gene duplication events in the ECE-*CYC2* gene lineage.

Acknowledgments

This work was supported in part by the Benjamin D. Hall, PhD & Margaret B. Hall Fund through the College of Liberal Arts and Sciences Research Excellence Initiative at the University of Kansas. And by the Botany Endowment fund to Ecology and Evolutionary Biology at the University of Kansas.

This project would not have been possible without the work of Vibhuti Singh for her help with initial construction of the RNAi vectors, Kaylee Livingston for her help with data collection, and Katie Sadler for her assistance in the greenhouse. A thank you to my committee members for their service and insightful remarks.

I want to thank my advisor Lena Hileman for all of her support and mentorship in research and my development as a plant biologist.

Table of Contents

INTRODUCTION

Overview of floral symmetry

The extensive diversity of angiosperms has long left naturalists pondering the form, function and evolution of complex floral structures (Friedman, 2009). Angiosperms rely on their flowers to both disperse and receive pollen for reproduction, but as sessile organisms, angiosperms have evolved various pollination strategies, often referred to as syndromes, to ensure cross-pollination (reviewed in Dellinger, 2020; Fenster et al., 2004). These include abiotic syndromes such as wind or water pollen dispersal, and a wealth of biotic syndromes such as dispersal by insects or birds. These abiotic and biotic interactions between flowers and pollen-transferring vectors introduce selection pressures that result in novel and complex floral traits, and therefore a wealth of diversity. To understand the processes underlying evolution of these diverse traits, we can now integrate phylogenetics, genetics and advanced molecular techniques to associate flower trait evolution with genetic and developmental mechanisms.

Extensive trait mapping on angiosperm phylogenies shows that parallel recruitment of adaptative floral traits is common across angiosperms. For example, fusion of floral organs (reviewed in Wessinger & Hileman, 2020), flower color (Wessinger et al., 2019), floral corolla tube length (Landis et al., 2018), or nectar spurs (Fernández-Mazuecos et al., 2019). One floral trait of interest that shows this pattern of parallel evolution is bilateral flower symmetry. Across angiosperms, we find two common forms of flower symmetry, radial and bilateral. Radial flower symmetry (polysymmetry, actinomorphy) is defined by having multiple axes of symmetry able to bisect a flower. Whereas, flowers with bilateral flower symmetry (monosymmetry, zygomorphy) have one axis of symmetry resulting in flowers with differentiated halves, dorsal (adaxial) and ventral (abaxial), with the single axis (dorsoventral axis) of symmetry vertical

along the flower (Figure 1). The ancestral form of floral symmetry has been determined to be radial through fossil and phylogenetic evidence (Dilcher, 2000; Sauquet et al., 2017) and has persisted in several extant linages (*e.g.* Nymphaeales, Oxalidales, Cornales) (Reyes et al., 2016). Yet, bilateral flower symmetry appeared early in the diversification of angiosperms (Magnoliids) (Reyes et al., 2016), with the first radiation occurring around the Paleocene and Eocene (Dilcher, 2000). Bilateral flower symmetry has been estimated to have evolved a minimum of 130 times across the angiosperm phylogeny with origins in all major linages (Reyes et al., 2016). In addition, reversals back to radial flower symmetry occurs in many lineages (Donoghue et al., 1998; Endress, 2012; Hileman, 2014; Ree & Donoghue, 1999; Reyes et al., 2016; Zhong et al., 2017). Large portions of floral diversity can be attributed to these repeated transitions between radial and bilateral flower symmetry and transitions are often associated with shifts in biotic pollinators (Neal et al., 1998; van der Niet & Johnson, 2012).

Figure 1. Floral symmetry forms commonly found in angiosperms, radial (A) and bilateral (B).

Strong selection with specialized pollinators is hypothesized to have driven the evolution of bilateral flower symmetry (Endress, 2001; Neal et al., 1998). Interactions among pollinator types and flowers differ between radially and bilaterally symmetric flowers (Rodriguez et al., 2004). Bilaterally symmetric flowers often have pollinator-specific features such as landing platforms (*i.e.* enlarged ventral petals), specialized reproductive organs (*e.g*. decrease in stamen number, curved styles and filaments), nectar guides (Endress, 1994), increases in corolla biomass (Herrera, 2009), and banner petals that either increase signaling or ability to transfer pollen (*i.e.* pollination success). These features promote plant-pollinator interactions and make them more efficient, thus often resulting in coevolution between pollinators and flowers (Fenster et al., 2004). Studies have demonstrated that bilaterally symmetric flowers more effectively direct pollinators compared to radially symmetric flowers, which can increase consistent pollen placement (Endress, 1999). The resulting increase in efficiency of pollen transfer ultimately improves the likelihood for cross-pollination thus leading to an increase in fitness (Gómez et al., 2006). Moreover, localized pollen placement may lead to reproductive isolation and potential speciation. Finally, bilateral flower symmetry has been shown to be associated with increases in net diversification rates (Sargent, 2004; Vamosi & Vamosi, 2010).

Genetics of bilateral flower symmetry in Lamiales

Gene and genome duplications are pervasive in plants. A survey of 41 land plant genomes found that on average 65% of plant genes are paralogous, with a high of 84% found in apple (*Malus domestica*) (Panchy et al., 2016). These duplications have contributed to the evolution of novel plant structures and forms (Flagel & Wendel, 2009), including in genes responsible for bilateral flower symmetry.

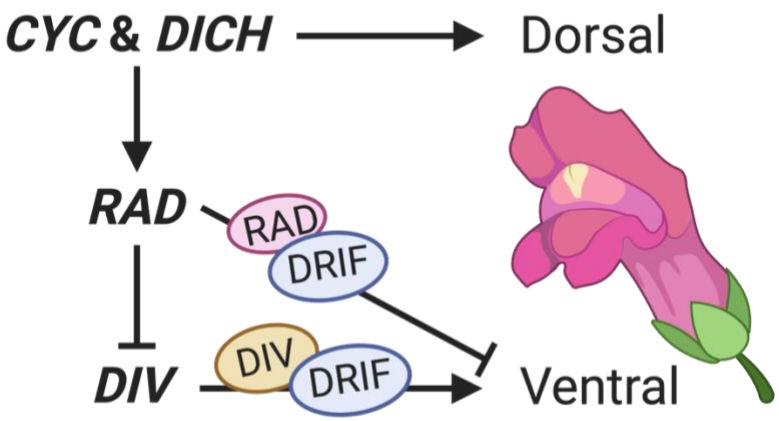

Figure 2. Bilateral flower symmetry genetic network as elucidated in *A. majus*. Arrows indicate positive regulation; line with a cross bar indicates repression. Created with BioRender.com.

The genetic program for bilateral flower symmetry has been well examined in the model system *Antirrhinum majus* (snapdragon, Order Lamiales) (Figure 2). *Antirrhinum majus* flowers are strongly bilateral, with two large dorsal petals comprising the dorsal region and two lateral petals flanking the ventral petal in the ventral region. Studies in this system have shown that while genome/gene duplications have produced numerous gene families, only two, though large, gene families are primarily responsible for bilateral flower symmetry: MYB (reviewed in Sengupta & Hileman, 2018) and TCP (reviewed in Martin-Trillo & Cubas, 2009) (and see below). Members of the TCP gene family, and key regulators of bilateral flower symmetry in *A. majus*, are the paralogs *CYCLOIDEA* (*CYC*) and *DICHOTOMA* (*DICH*). *CYC* and *DICH* have partially redundant functions in establishing dorsal flower identity in *A. majus* (Luo et al., 1996, 1999). The roles of these genes differ slightly in that *CYC* functions to establish overall dorsal flower identity and abortion of the dorsal stamen (Luo et al., 1996), while *DICH* functions to specifically establish dorsal petal identity (Luo et al., 1999). Evidence from the infamous *A. majus* mutants show that only in the *cyc*;*dich* double mutant is the flower fully radialized (Luo et al., 1999). *CYC* and *DICH* are understood to regulate cell-cycle genes (reviewed in Martin-Trillo & Cubas, 2009), controlling growth. However, it is unclear what regulators may be upstream of

these dorsal identity genes. Some evidence suggests plant hormones may play a role in regulating *CYC* and *DICH*. For example, the addition of auxin to *A. majus* flowers resulted in radialized flowers (Bergbusch, 1999).

CYC and *DICH* positively regulate *RADIALIS* (*RAD*), a transcription factor in the MYB gene family (Corley et al., 2005). *RAD* restricts ventral identity to the ventral region of the flower by inhibiting the activity of *DIVARACATA* (*DIV*) in the dorsal region (Corley et al., 2005) (Figure 2). *DIV*, also a MYB transcription factor, is responsible for activating ventral petal identity genes (Almeida et al., 1997; Galego & Almeida, 2002). DIV relies on the binding of DIV-and-RAD-interacting-factors (DRIF), a pair of MYB proteins. DIV and DRIF form a heterodimer complex capable of DNA binding (Raimundo et al., 2013). However, RAD proteins also bind to DRIF proteins and when RAD proteins are present they outcompete DIV for DRIF binding (Figure 2). This prevents the formation of the DRIF-DIV complex and suppresses ventral identity in the dorsal region (Raimundo et al., 2013). *CYC*, *DICH* and *RAD* expression is constrained to the dorsal region of the flower (Corley et al., 2005; Luo et al., 1996, 1999), allowing the DRIF-DIV complex to fully function in the ventral region. RAD proteins are found in the margins of the lateral petals, but presumably via nonautomous movement of mRNA or protein from the dorsal region (Corley et al., 2005). Lateral petal identity is thereby hypothesized to have marginal control by RAD, where petal shape is a combination of dorsal and ventral petal traits (Corley et al., 2005). Alternatively, lateral petal form is the default as shown in the *cyc*;*dich*;*div A. majus* mutant, which presents flowers comprised solely of lateral petals, additionally, in *div* mutants, the ventral petal takes on lateral identity (Almeida et al., 1997).

Since the elucidation of the developmental program of bilateral flower symmetry in *A. majus*, researchers have been exploring floral symmetry genes in non-model systems of other

Asterids as well as clades in Rosids, monocots, and basal eudicots (Broholm et al., 2008; Busch & Zachgo, 2007; Citerne et al., 2017; Feng et al., 2006; Garcês et al., 2016; Jabbour et al., 2014; Madrigal et al., 2019; Wang et al., 2008). They have found parallel recruitment of *CYC* and *MYB* genes for establishing bilateral flower symmetry in many of these clades, although operating under differing developmental mechanisms.

Evolutionary history of *CYC*-like genes

CYC and *DICH* are members of TCP, a large plant-specific gene family of transcription factors. The name TCP originates from four genes within the family: *TEOSINTE BRANCHED1* (*TB1*) (maize; Doebley et al., 1997), *CYC* (snapdragon; Luo et al., 1996), and *PROLIFERATING CELL FACTORS 1* and *2* (*PCF1* and *PCF2*) (rice; Kosugi & Ohashi, 1997). A conserved trait shared by members of TCP is the TCP domain, a basic helix-loop-helix composed of 59-amino acids capable of DNA binding and protein-protein interactions (Cubas et al., 1999). Proteins in this family have been documented to be involved in developmental control of plant morphology by both promoting (Hervé et al., 2009; Li et al., 2005) and inhibiting (Feng et al., 2006; Luo et al., 1996) cell proliferation and growth.

Repeated duplications within the TCP family have resulted in two major linages of TCP genes, class I and class II, with the class II subfamily containing a conserved R domain (arginine-rich motif) (Cubas et al., 1999). A subset of this class II lineage contains an additional conserved domain, the ECE (glutamic acid-cysteine-glutamic acid) motif (Howarth & Donoghue, 2006). Extensive independent duplications of the ECE lineage have occurred during angiosperm diversification. Two specific duplications of the ECE clade gave rise to three gene groups shared by the core eudicots (Howarth & Donoghue, 2006): *CYC1*, *CYC2*, and *CYC3*, and multiple copies of each of these three gene groups are found in core eudicots (Citerne et al.,

2003; Hileman et al., 2003; Reeves & Olmstead, 2003). Similarly, often more than one ECE *CYC*-like gene is found in monocots and basal eudicots (Bartlett & Specht, 2011; Citerne et al., 2013). Within the ECE clade, ECE-*CYC2* is the parent lineage of *CYC* and *DICH*. ECE-*CYC2* genes (including *CYC* and *DICH*) have been shown to control cell cycle and organ differentiation, in many cases by preventing cell proliferation (Luo et al., 1996). ECE-*CYC*2 genes tightly control mRNA distribution by maintaining localized patterning specific to development and tissue type.

At least five core eudicot groups (Brassicales, Malpighiales, Dipsacales, Asterales, and Lamiales) show a repeated pattern of duplication linked to recruitment of ECE-*CYC2* genes for bilateral flower symmetry development (reviewed in Hileman, 2014). This is supported by phylogenic and expression evidence (Bartlett & Specht, 2011; Busch et al., 2012; Citerne et al., 2006, 2017; Howarth et al., 2011; Howarth & Donoghue, 2005; Hsin et al., 2019; Hsin & Wang, 2018; Jabbour et al., 2014; Pang et al., 2010; Preston et al., 2011; Preston & Hileman, 2012; Zhang et al., 2010, 2012, 2013; Zhao et al., 2019; Zhong et al., 2017; Zhong & Kellogg, 2015a, 2015b; Zhou et al., 2008), in addition to functional evidence in a small number of studies (Broholm et al., 2008; Busch & Zachgo, 2007; Feng et al., 2006; Garcês et al., 2016; Juntheikki-Palovaara et al., 2014; Preston et al., 2014; Wang et al., 2010; Wang et al., 2008; Xu et al., 2013; Zhao et al., 2018). Duplication of ECE-*CYC2* genes is often followed by spacio-temporal changes in expression, which can result in sub- and neofunctionalization of resulting paralogs (Preston & Hileman, 2009; Spencer & Kim, 2017). In Fabales for example, ECE-*CYC2* duplications and functional divergence are linked to the establishment of bilateral flower symmetry in Papilionoideae (Zhao et al., 2019). In sunflowers, several duplications of the ECE-*CYC2* group resulted in at least five gene members and, followed by sub- and

neofunctionalization, expression of only one of the five ECE-*CYC2* genes is restricted to the bilaterally symmetric ray florets (Chapman et al., 2008). Similar patterns hold for Malpighiales (Zhang et al., 2010) and Dipsacales (Howarth & Donoghue, 2005).

Less well explored are comparative functional studies of ECE-*CYC2* lineage paralogs within angiosperm lineages where bilateral flower symmetry is dominant. Specifically, we lack a comprehensive understanding of how bilateral flower symmetry is maintained following duplication in the ECE-*CYC2* gene lineage. For example, in *A. majus CYC* and *DICH* are paralogs derived from a recent duplication event (Gübitz, 2003; Hileman & Baum, 2003); *CYC* maintains most of the presumed ancestral function of specifying dorsal flower organ identity while *DICH* primarily functions to shape the dorsal petals (Luo et al., 1996, 1999). Is this evolutionary progression common? One paralog primarily maintaining the overall dorsal flower organ identity function while the other paralog, if retained, evolves a novel function? Addressing these outstanding questions provides an opportunity to study evolutionary change in gene networks during the maintenance of key adaptive phenotypes (*e.g.* bilateral flower symmetry).

Study system

Bilateral flower symmetry evolved early in the order Lamiales and has been retained in most lineages except a few in which there have been reversals to radial symmetry (Donoghue et al., 1998; Preston et al., 2011; Zhong & Kellogg, 2015a). Yet during Lamiales diversification, the ECE-*CYC2* gene lineage has been estimated to have undergone at least 13 gene duplications (Zhong & Kellogg, 2015b) (Figure 3). Maintenance of Lamiales ECE-*CYC2* lineage paralogs is surprising given the high level of bilateral flower symmetry conservation across the group. One of these duplications occurred at the base of Antirrhineae (Plantaginaceae), resulting in the paralogs *CYC* and *DICH* (Gübitz et al., 2003; Hileman & Baum, 2003). Another set of paralogs

is shared by the Higher Core Lamiales (HCL) clade, HCL-*CYC2A* and HCL-*CYC2B* (Zhong & Kellogg, 2015b). These independent gene duplication events provide an opportunity to test for shared patterns of functional evolution following duplication when overall associated morphology is conserved—bilateral flower symmetry in this example.

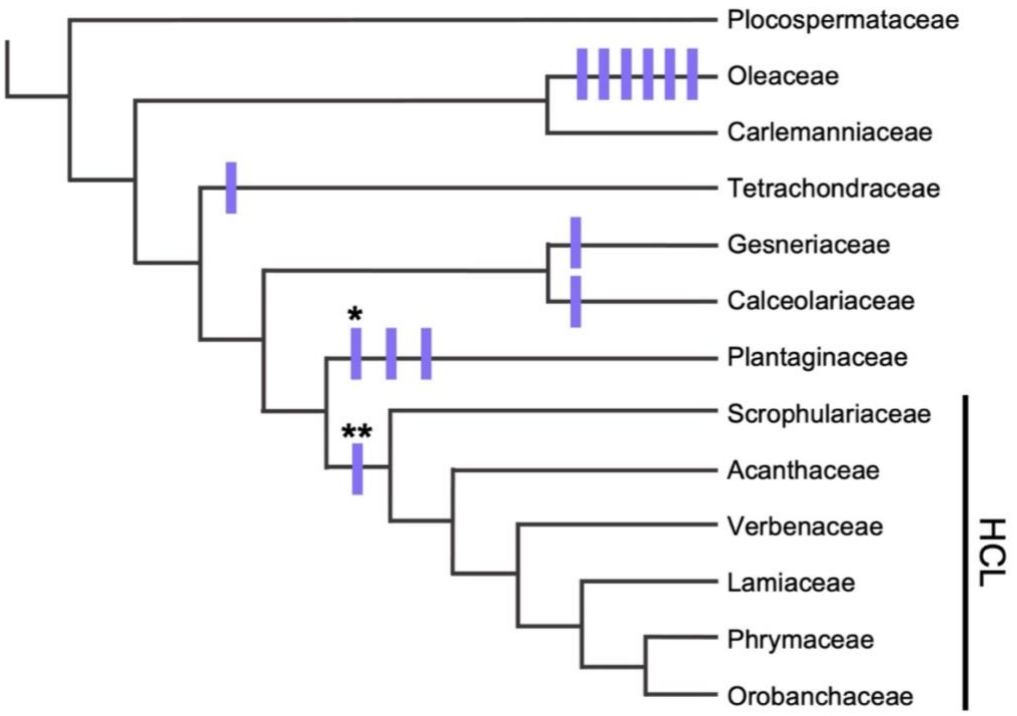

Figure 3. Cladogram of Lamiales depicting the duplication events of the ECE-*CYC2* gene lineage proposed by Zhong and Kellogg (2015b) as indicated by purple tick marks. *indicates duplication that gave rise to *CYC* and *DICH*; **indicates duplication that gave rise to HCL-*CYC2A* and HCL-*CYC2B* shared by the Higher Core Lamiales (HCL).

Mimulus (Phrymaceae, belonging to the HCL group) is a prominent system for investigating ecological and evolutionary questions, and has more recently been expanded as a model system in genetic and developmental studies (Yuan, 2018). Specifically, *Mimulus lewisii* is an emerging model, complete with a draft genome (www.mimubase.org) and rigorous protocols for transient (Ding & Yuan, 2016) and stable (Yuan, Sagawa, Young, et al., 2013) transformation. Several studies have demonstrated that stable transgenic RNAi experiments

produce proof for forward genetics and allow for examination of gene function in *M. lewisii* (LaFountain et al., 2017; Sagawa et al., 2016; Yuan, Sagawa, Stillo, et al., 2013; Yuan, Sagawa, Young, et al., 2013). The focus of these transgenic RNAi experiments has been on pigment biosynthesis and corolla tube formation, however, functional studies investigating the flower symmetry genetic network have not been published for *M. lewisii*.

Functional studies in *Mimulus guttatus* investigating the HCL-*CYC2A* (*MgCYC2*) and HCL-*CYC2B* (*MgCYC1*) paralogs (Preston et al., 2014) suggested partially redundant functions. Specifically, loss of flower dorsal identity was only seen in double silenced *MgCYC1*:*MgCYC2*. However, Preston *et al.* (2014) utilized a Virus-Induced Gene Silencing (VIGS) approach to ECE-*CYC2* lineage gene downregulation. VIGS is highly variable, even within a single flower, and therefore gene function for individual paralogs was not fully determined. With the continued improvement of a genome, rigorous stable transformation protocol, and placement in the HCL, *M. lewisii* is an optimal study system to investigate the genetic program of bilateral flower symmetry. Specifically, with focus on the HCL-*CYC2A* and HCL-*CYC2B* paralogs and the potential for a comparative framework with *A. majus*.

Here, we test for the conservation of the bilateral symmetry development program in *M. lewisii* as compared to *A. majus*. We survey the expression of HCL-*CYC2B* (*MlCYC1*), HCL-*CYC2A* (*MlCYC2*), *MlRAD4*, and *MlRAD5* across floral development and between floral tissue types to determine patterns consistent with a role in establishing dorsal flower identity. We use stable transgenic experiments to investigate the paralog-specific and combined functions of *MlCYC1* and *MlCYC2*. With these methodologies we address the following questions: 1) What are the respective roles of *MlCYC1* and *MlCYC2* in *M. lewisii* bilateral flower symmetry development? 2) Do *MlCYC1* and/or *MlCYC2* positively regulate *MlRAD*?

MATERIALS AND METHODS

Plant Growth Methods

Mimulus lewisii FL10 seeds (Yuan, Sagawa, Young, et al., 2013) were provided by Yaowu Yuan (University of Connecticut). Berger BM7HP (Berger) soil medium was used for all plant propagation. We grew all plants in climate-controlled growth chambers at the University of Kansas under KIND LED X-80 Bar Lights (KIND LED Grow Lights), with a long day photoperiod (16-h light/8-h dark), and 21/15°C day/night temperature cycles. We stratified sowed seeds at 4°C for 5-7 days. We then placed the sowed seeds under Vegetative Bar Lights (blue-spectrum) for germination, moving them to Flower Bar Lights (blue- and red-spectrum) at approximately the 4-leaf stage. Once mature, we maintained plants under Flower Bar Lights, hand watered and fertilized with Blossom Booster (Peters Professional, Scotts) approximately every two weeks.

DNA Methods / DNA Extractions

From young leaf tissue, we extracted genomic DNA (gDNA) using the Cetyltrimethylammonium bromide (CTAB) method (Doyle & Doyle, 1987). We ground liquid nitrogen flash-frozen leaf tissue to a fine powder using a chilled mortal with pestle. The ground tissue from each sample was transferred into 600 µl CTAB buffer (1M Tris-HCl pH 8, 5M NaCl, 0.5M EDTA pH 8, CTAB, milliQ H_2O) with 100 mg/ml PVP, 4.4 mg/ml ascorbic acid, and 20 µl/ml 2M DTT and digested for 1-h at 60°C. We purified gDNA with 24:1 chloroform-isoamyl. In addition, we performed an RNase treatment by adding 5 µl PureLink RNase A 20mg/ml (Invitrogen) in 500 µl extracted gDNA, and incubating for 30-60 min at 37°C. gDNA was purified with an additional wash of 24:1 chloroform-isoamyl. We precipitated gDNA in

isopropanol at -20°C for 20 min. gDNA was pelleted, washed x2 with 70% ethanol, and eluted in low Tris EDTA buffer. gDNA was stored at -20°C.

RNA Methods / RNA Extractions and cDNA Synthesis

Liquid nitrogen flash-frozen plant tissues were ground to a fine powder as above. We extracted total RNA from plant tissues using the RNeasy Plant Mini Kit (QIAGEN) following manufacturer's protocol. We removed residual DNA with the TURBO DNA-*free* Kit (Invitrogen) following manufacturer's protocol. RNA was stored at -80°C. From our isolated RNA, we synthesized complementary DNA (cDNA) using the High-Capacity cDNA Reverse Transcription Kit (Applied Biosystems) following manufacturer's protocol. cDNA was stored at -20°C.

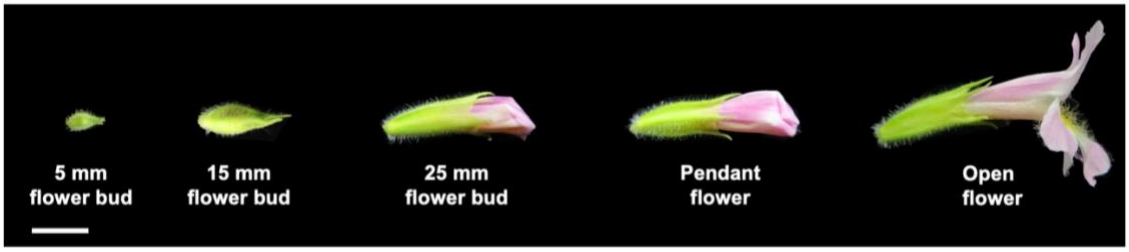

Figure 4. Flower developmental stages selected for expression analyses, (scale bar, 1 cm).

qRT-PCR Qualitative Expression / Developmental stages

We performed quantitative reverse transcriptase PCR (qRT-PCR) to determine the expression patterns of *MlCYC1*, *MlCYC2*, *MlRAD4*, and *MlRAD5* across flower development in *M. lewisii* LF10. We collected whole flower buds for five flower developmental stages (5 mm, 15 mm, 25 mm, pendant, open; Figure 4), leaf, and stem node tissues. We isolated flower organs (sepals, petals, stamens, carpels) for the 15 mm and pendant flower developmental stages; isolated organs were pooled from four flowers. We isolated ventral and dorsal specific floral tissues for the 5 mm, 15 mm, and open flower developmental stages; isolated tissues were pooled

from four flowers for the 5 mm flower bud stage. Collected tissues were flash frozen immediately following collection and stored at -80°C. From these tissues, we isolated total RNA, purified, and synthesized to cDNA as described in RNA methods. With a real-time PCR instrument (QuantStudio®3, Applied Biosystems), we amplified and quantified each gene fragment from cDNA (diluted 1:20 as template for qRT-PCR reactions) using gene-specific primers (Table A1) and PowerUp SYBR Green Master Mix (Applied Biosystems) following manufacturer's protocol. We normalized the expression of *MlCYC1*, *MlCYC2*, *MlRAD4* and *MlRAD5* with the expression of *MlIFA* (transcription initiation factor TFIID subunit 2) (Stanton et al., 2017). We calculated relative expression for each gene, developmental stage, and tissue type using the ΔΔCt method with primer amplification efficiency correction (Peirson et al., 2003).

RNAi Plasmid Construction

Following Yuan *et al.* (2013a), we built independent RNA interference (RNAi) binary vectors for expression knockdown of *MlCYC1* and *MlCYC2* in *M. lewisii* LF10. We targeted and amplified gene fragments from *MlCYC1* (274-bp) and *MlCYC2* (157-bp) (Figure A1) from cDNA using Phusion High-Fidelity DNA Polymerase (New England Biolabs) and primer pairs with restriction sites for cloning (Table A2). Amplified *MlCYC1* and *MICYC2* fragments were digested and each inserted, respectively, into the binary vector pFGC5941 (Kerschen et al., 2004; Arabidopsis Biological Resources Center, CD3-447) as follows. First, amplified fragments were cloned into the pFGC5941 vector in the sense orientation at the *AscI*/*NcoI* site. Next, the same amplified fragment was cloned in the antisense orientation at the *BamHI*/*XbaI* site of the vector containing the sense fragment. We sequenced the final plasmids to verify correct gene fragment

and placement in each plasmid. We transformed *Agrobacterium tumefaciens* (strain GV3103) by electroporation with our final *MlCYC1* and *MlCYC2* RNAi binary vectors.

Agrobacterium-mediated Plant Transformation

To test the function of *MlCYC1* and *MlCYC2* we generated transgenic lines carrying the T-DNA insert from our binary vectors. We followed the protocol for stable transformation of *M. lewisii* LF10 (Yuan, Sagawa, Young, et al., 2013). This method includes both floral spray and vacuum infiltration. We grew transformed *A. tumefaciens* to stationary phase in liquid culture at 29°C in sterilized LB with rifamycin (25 mg/L), kanamycin (50 mg/L), and gentamycin (50 mg/L). We aggregated the bacteria from the culture by centrifuging for 15-20 min at 4°C and 4000 rpm and resuspended the cells in an inoculation solution (milliQ water, 5% sucrose, 0.1M acetosyringone, and 1ml/L Silwett (Vac-n-stuff)). Wild-type plants were trimmed to induce lateral growth in order to increase overall abundance of floral meristems. We selected plants with large quantities of young flower buds (< 5 mm) for inoculation and removed larger flower buds. We heavily sprayed flower buds with transformed *A. tumefaciens* resuspended in inoculation solution, placed plants inside a pressure chamber and vacuum infiltrated plants for two minutes at 26-28 Hg, followed by a quick release of pressure. Inoculated plants were housed inside a dark, humid box to recuperate for a 24-h period, then placed back in a growth chamber under the Flower Bar Lights. We self-pollinated infiltrated flowers at a whole plant level for two weeks and collected fruits 2-3 weeks after pollination for a 1-2 week period.

Transgenic Plant Confirmation

Selection of transgenic plants is possible since the T-DNA from the pFGC5941 vector contains the *BAR* gene, which provides resistance to glufosinate, an herbicide compound. Seeds collected from inoculated flowers were sown on flats of soil and grown as described for plants

above. To select for transgenics, we sprayed seedlings with BASTA (glufosinate ammonium, 1:1000, Bayer CropScience) every 2-3 days for a total of 5 sprays. Putative transgenic lines were transplanted into individual pots and screened for the transgene via PCR: two primer pairs, pFGC5941_2372F/3082R and pFGC5941_3930F/4430R specific to vector regions flanking the insert (Table A3), were used to confirm that the complete RNAi T-DNA fragment was inserted, which is necessary to produce the hairpin RNA (hpRNA).

Confirmation of *MlCYC1* and *MlCYC2* Expression Downregulation in RNAi Lines

To confirm that *MlCYC1* and *MlCYC2* RNAi lines were demonstrating downregulation of the respective gene, we utilized qRT-PCR. The 15 mm flower bud developmental stage was selected for expression analysis based on the relatively high level and low variation in *MlCYC1* and *MlCYC2* expression at this stage in wild-type *M. lewisii* LF10 plants. From whole 15 mm flower buds, RNA was extracted, purified, and synthesized to cDNA as described in RNA Methods. We amplified and quantified *MlCYC1* and *MlCYC2* transcripts using qRT-PCR methods as described above.

***MlCYC1*:*MlCYC2* RNAi Line Generation**

To generate *MlCYC1*:*MlCYC2* double RNAi lines, we selected *MlCYC1*_RNAi and *MlCYC2*_RNAi lines confirmed for downregulation and cross-pollinated them to produce a variety of independent lines. We collected seeds and grew plants as described in Plant Growth Methods. Seeds were initially screened for transgenic plants using BASTA (glufosinate ammonium, 1:1000, Bayer CropScience). To confirm the presence of at least one of the respective *MlCYC1* and *MlCYC2* T-DNA inserts, we isolated gDNA as described in DNA Methods and performed PCR using primers specific to each *MlCYC1* and *MlCYC2* RNAi T-DNA (Table A4). Plants confirmed to carry both *MlCYC1* and *MlCYC2* RNAi T-DNA inserts

were further confirmed for both *MlCYC1* and *MlCYC2* gene expression knockdown by qRT-PCR methods as described above.

RNAi Line Characterization

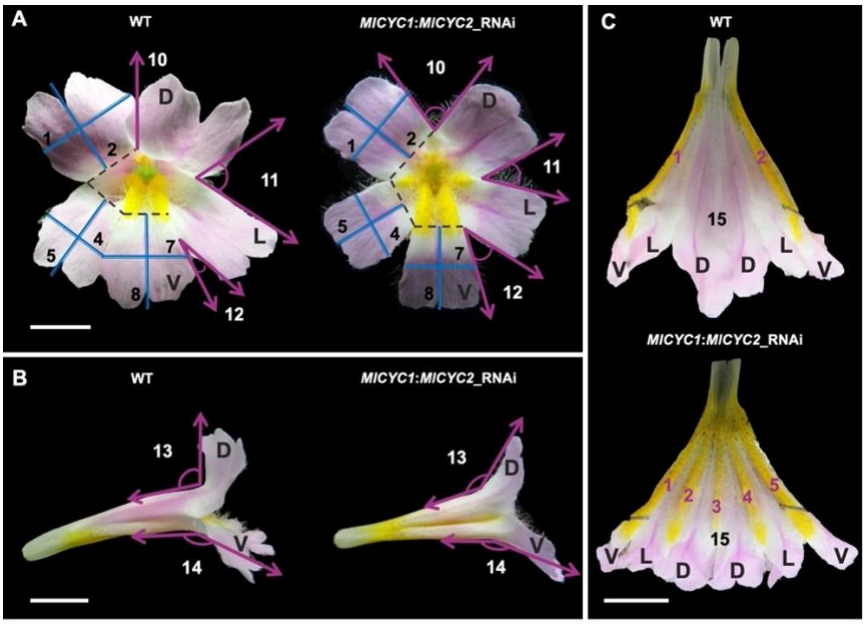

Figure 5. Diagram of flower traits measured for wild-type and all RNAi lines. Face view measurements taken shown on wild-type and *MlCYC1*:*MlCYC2*_RNAi flowers (A), (scale bar, 1 cm). Side view of measurements taken shown on wild-type and *MlCYC1*:*MlCYC2*_RNAi flowers (B), (scale bar, 1 cm). Dissected corolla tube with nectar guide ridge counts on wild-type and *MlCYC1*:*MlCYC2*_RNAi flowers (C), (scale bar, 1 cm). Numbers correspond to character ID traits listed in Table 1. D, dorsal petal; L, lateral petal; V, ventral petal.

Table 1. Flower traits measured for characterization of RNAi lines. Character IDs correspond to diagram (Figure 5).

Character ID	Flower viewpoint	Description	Details
1	Face	Dorsal petal width	cm; petals averaged
2	Face	Dorsal petal length	cm; petals averaged
3	Face	Dorsal petal width:length	ratio
4	Face	Lateral petal width	cm; petals averaged
5	Face	Lateral petal length	cm; petals averaged
6	Face	Lateral petal width:length	ratio
7	Face	Ventral petal width	cm
8	Face	Ventral petal length	cm
9	Face	Ventral petal width:length	ratio
10	Face	Dorsal-dorsal petal angle	Deg.
11	Face	Dorsal-lateral petal angle	Deg.; angles averaged
12	Face	Ventral-lateral petal angle	Deg.; angles averaged
13	Side	Dorsal corolla tube flare	Deg.
14	Side	Ventral corolla tube flare	Deg.
15	Dissected	Nectar guide ridge count	WT=2; half scores given; includes presence of anthocyanin spots, trichomes, and carotenoid pigment

To determine changes in flower morphology we characterized floral phenotypes of *MlCYC1, MlCYC2* and *MlCYC1:MlCYC2* RNAi lines. When possible, we collected the first several flowers at anthesis and photographed each flower from multiple viewpoints on a scaled stage. To photograph the inner corolla tube, we dissected flowers along the center of the ventral petal between the two nectar guide ridges. 15 floral traits (Figure 5; Table 1) were measured using Fiji (https://imagej.net/Fiji). Each measurement was taken 3x and we recorded the mean. For flower petal shape, we took the width to length ratio to account for high plasticity in overall flower size. To test for significance, we performed a two-tailed, unpaired Student's T-test for each trait between *M. lewisii* LF10 plants compared to each independent RNAi line.

Quantitative Expression of *MlRAD5* in RNAi Lines

We performed qRT-PCR to test for downregulation of *MlRAD5* in the *MlCYC1*:*MlCYC2* RNAi backgrounds. From 15 mm flower buds, we isolated petal+attached stamen and carpel organs; isolated organs were pooled from four flowers per plant. Pools were collected from wild-type (*n*=4) and *MlCYC1*:*MlCYC2*_RNAi lines (*n*=19). For each pool, we extracted and purified RNA and synthesized cDNA as described in RNA methods. We amplified and quantified *MlRAD5* transcripts using gene specific primers (Table A1) and qRT-PCR methods as described above.

Identifying *M. lewisii CYC* orthologs

Putative *M. lewisii CYC* orthologs were identified in Sengupta and Hileman (2018): *Mimulus_lewisii_CYCLOIDEA*_like_2a_sc424_contig9407 (here *MlCYC1*) and *Mimulus_lewisii_CYCLOIDEA*_like_2b_sc2324_contig13781 (here *MlCYC2*). We recovered coding sequences for these genes from the *M. lewisii* LF10 draft genome (www.mimubase.org) and aligned them manually to known HCL *CYC2A* and *CYC2B* lineage genes (Figure A1; Table

A5) in Geneious Prime v.2021.2.2. We used these alignments to estimate gene relationships under Maximum Likelihood, GTR+Gamma model of molecular evolution in RAxML (Stamatakis, 2006) implementing 1000 bootstrap replicates.

RESULTS

MlCYC1 and *MlCYC2* belong to the higher core Lamiales *CYC2B* and *CYC2A* lineages, respectively

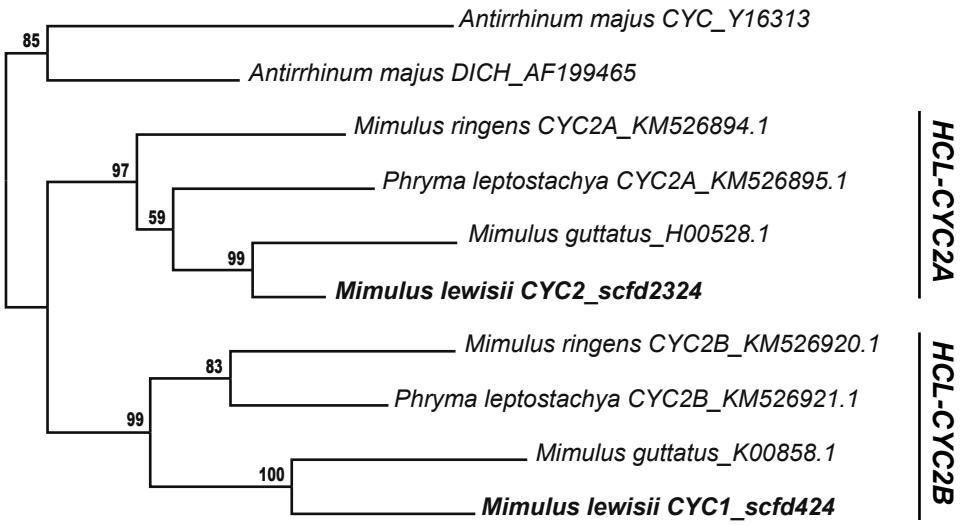

Figure 6. Maximum likelihood ECE-*CYC2* gene tree reconstructed via RAxML with 1000 bootstrap replications. Numbers at nodes indicate recovered bootstrap support. Labels at right indicate HCL-*CYC2A* and HCL-*CYC2B* gene lineages, respectively.

We included *MlCYC1* and *MlCYC2* in a phylogenetic analysis with other *CYC2*-lineage genes from Phrymaceae (HCL; Zhong & Kellogg, 2015b) rooted with *A. majus CYC* and *DICH* (Luo et al., 1996, 1999). We found that *MlCYC1* belongs to the HCL-*CYC2B* lineage (97% bootstrap support) and *MlCYC2* belongs to the HCL-*CYC2A* lineage (99% bootstrap support; Figure 6). Therefore, the duplication that gave rise to *MlCYC1* and *MlCYC2* paralogs is quite ancient, dating to before the diversification of the HCL clade (Zhong & Kellogg, 2015b).

MlCYC1 and *MlCYC2* show dorsal perianth expression with additional *MlCYC1* carpel expression

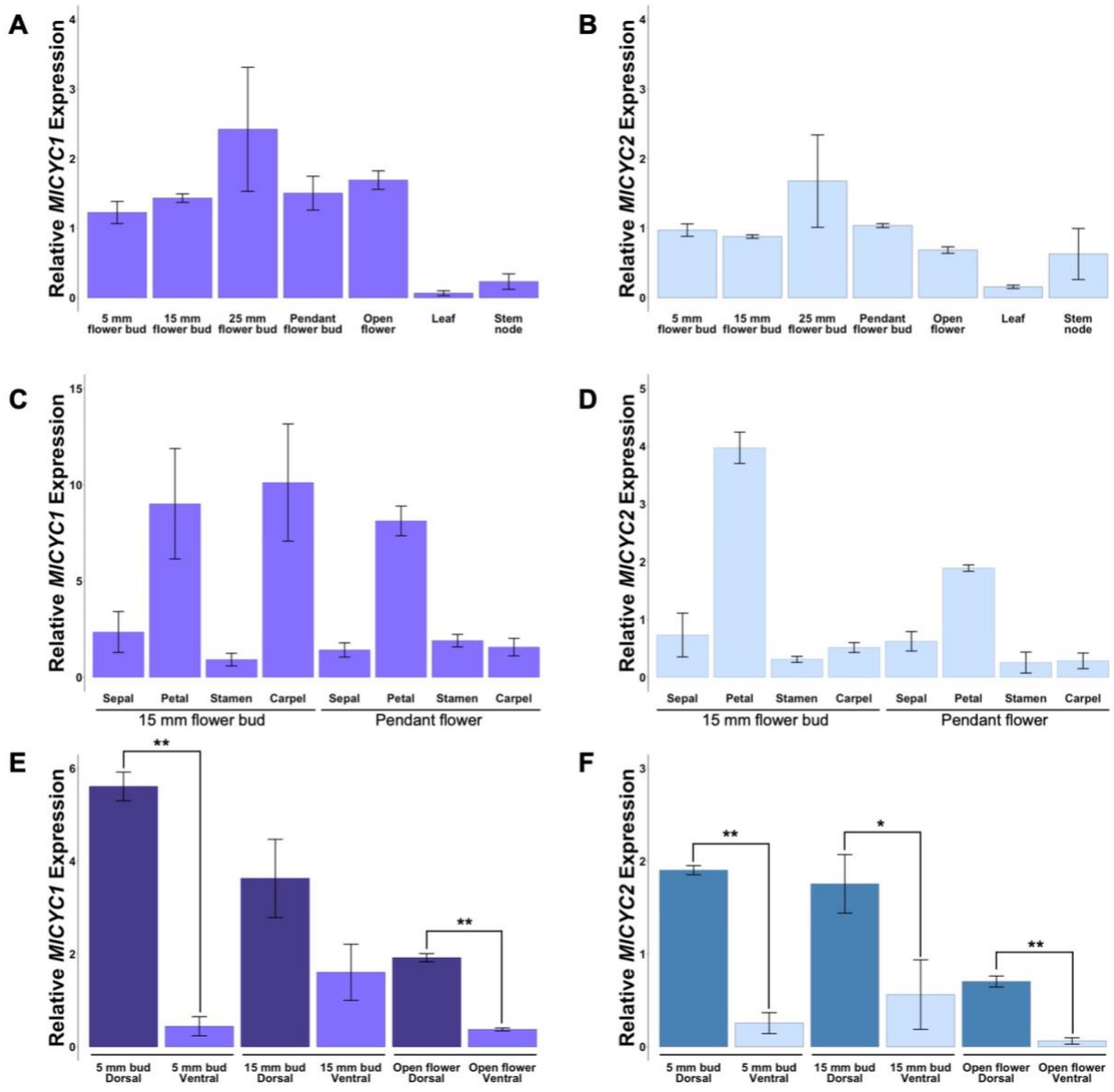

Figure 7. Relative expression of *MlCYC1* and *MlCYC2* across flower developmental stages and floral tissue types in *M. lewisii* LF10. Relative expression of *MlCYC1* (A) and *MlCYC2* (B) in whole flowers (15 mm to anthesis), leaves and node sections of stems. Relative expression of *MlCYC1* (C) and *MlCYC2* (D) across floral organs (sepals, petals, stamens and carpels) at two developmental stages (15 mm flower buds and pre-anthesis pendant flowers). Relative expression of *MlCYC1* (E) and *MlCYC2* (F) in dorsal compared to ventral halves of flowers at three developmental stages (5 mm flower bud, 15 mm flower bud, and flowers at anthesis), color shading indicates dorsal (darker) and ventral (lighter) samples. All tissues were normalized to the 5 mm whole flower bud stage. (T-test; *, 5% significance level; **, 1% significance level).

We performed qRT-PCR to determine the patterns of *MlCYC1* and *MlCYC2* expression across flower development in *M. lewisii* LF10. We selected five developmental stages that broadly span early to late flower development (5 mm, 15 mm, and 25 mm flower buds, pendant flowers just before anthesis, and open flowers at anthesis). In addition to flowers, we included leaf and stem node tissues. Across flower development, *MlCYC1* and *MlCYC2* showed similar patterns of relative expression (Figure 7). We found expression of both genes at early stages of development (5 mm), persisting to anthesis with both paralogs peaking in expression at the 25 mm flower bud stage (Figure 7A, B). Levels of relative expression of *MlCYC1* in leaf and stem node tissue are negligible (Figure 7A). Levels of relative expression of *MlCYC2* are similarly negligible in leaf tissue, however, low *MlCYC2* expression was observed in stem node tissue (Figure 7B).

We expanded floral expression comparisons of *MlCYC1* and *MlCYC2* to determine expression patterns specific to floral organs (sepals, petals, stamens, and carpels) for two developmental stages (15 mm flower buds and pendant flowers). We found high expression of *MlCYC1* and *MlCYC2* in petal tissue at both developmental stages (Figure 7C, D). The relative expression of *MlCYC2* decreased in petals at the pendant flower stage (Figure 7D), while *MlCYC1* maintained higher relative expression at this stage (Figure 7C). We observe a striking difference in carpel expression between paralogs. In 15 mm flower buds, *MlCYC1* displayed high expression in carpel tissue, with a drastic decrease in expression at the pendant flower stage (Figure 7C). By contrast, *MlCYC2* displayed low to negligible expression in carpels at both stages (Figure 7D). Both *MlCYC1* and *MlCYC2* showed low expression in sepals and stamens at both developmental stages (Figure 7C, D).

To determine if *MlCYC1* and *MlCYC2* expression is restricted to the dorsal region of developing flowers, we isolated dorsal and ventral floral tissues from 5 mm flower buds, 15 mm flower buds and from flowers at anthesis. We found that both *MlCYC1* and *MlCYC2* have significantly higher expression in dorsal tissues at most stages of development (*MlCYC1*: 5 mm, $P = 8.7 \times 10^{-6}$; 15 mm, $P = 0.099$; anthesis, $P = 3.1 \times 10^{-6}$; *MlCYC2*: 5 mm, $P = 1.1 \times 10^{-5}$; 15 mm, $p = 0.050$; anthesis, $P = 8.2 \times 10^{-5}$; Figure 7E, F). Expression of both *MlCYC1* and *MlCYC2* was variable in ventral tissues across different stages of development. However, most stages exhibited very low expression except *MlCYC1* at the 15 mm stage (Figure 7E), which was not significantly different from dorsal expression (Figure 7E). This relatively higher level of *MlCYC1* expression in 15 mm ventral flower buds may be due to relatively high but likely symmetric *MlCYC1* expression in same stage carpels (Figure 7C).

MlRAD5 but not *MlRAD4* shows dorsal perianth expression with additional carpel expression

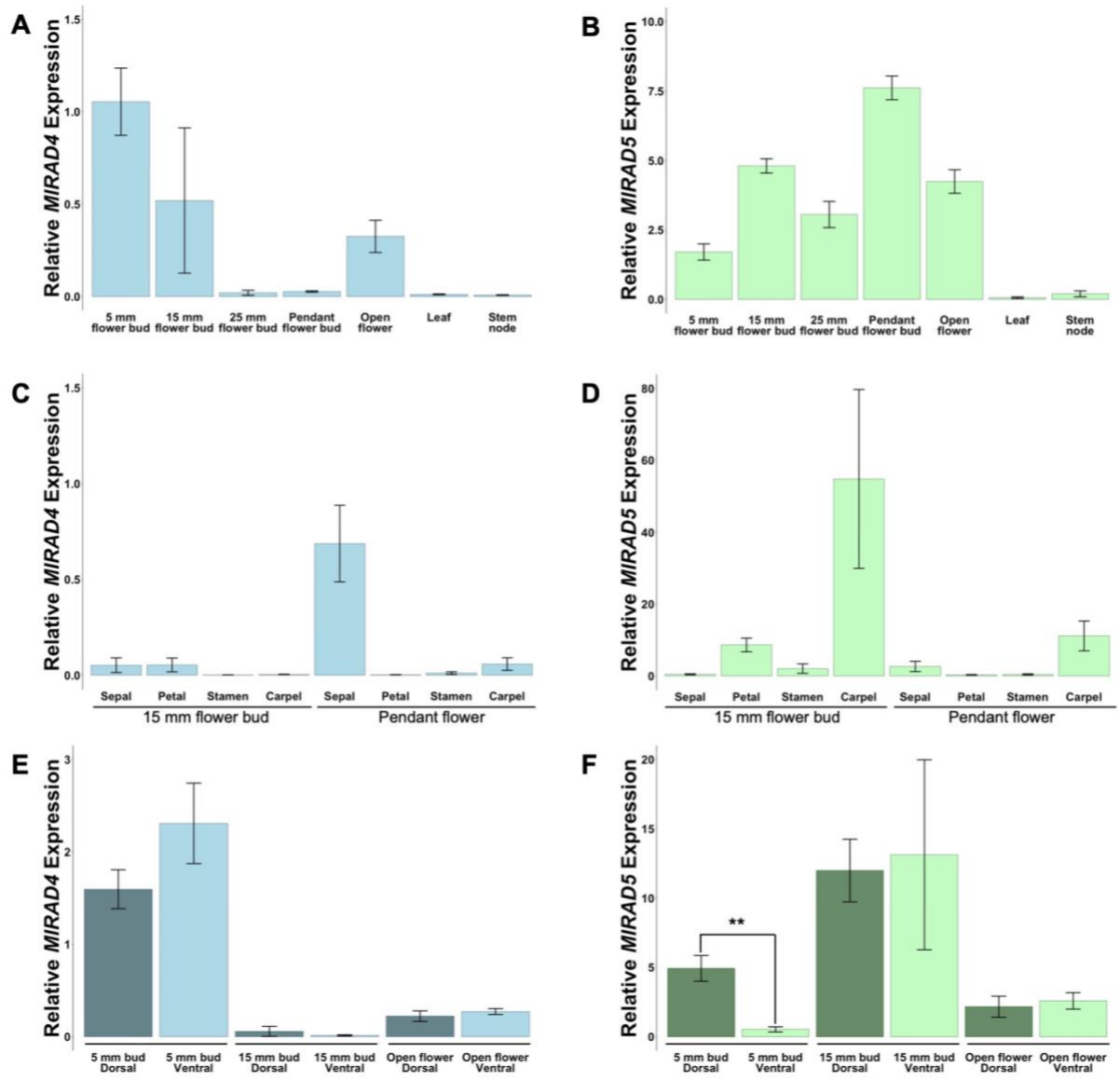

Figure 8. Relative expression of *MlRAD4* and *MlRAD5* across flower developmental stages and floral tissue types in *M. lewisii* LF10. Relative expression of *MlRAD4* (A) and *MlRAD5* (B) in whole flowers (15 mm to anthesis), leaves and node sections of stems. Relative expression of *MlRAD4* (C) and *MlRAD5* (D) across floral organs (sepals, petals, stamens and carpels) at two developmental stages (15 mm flower buds and pre-anthesis pendant flowers). Relative expression of *MlRAD4* (E) and *MlRAD5* (F) in dorsal compared to ventral halves of flowers at three developmental stages (5 mm flower bud, 15 mm flower bud, and flowers at anthesis), color shading indicates dorsal (darker) and ventral (lighter) samples. All tissues were normalized to the 5 mm whole flower bud stage. (T-test; *, 5% significance level; **, 1% significance level).

MlRAD4 and *MlRAD5* are the closest *M. lewisii* homologs to *A. majus RAD* (Sengupta & Hileman, 2018). We performed qRT-PCR to determine the patterns of *MlRAD4* and *MlRAD5* expression across flower development in *M. lewisii* LF10, and to determine which *RAD* paralog (or both) likely functions similarly to *A. majus RAD* in regulating bilateral flower symmetry. We used the same tissue samples as described for *MlCYC* expression analyses. We found that *MlRAD5* is expressed from early through late stages of flower development (Figure 8B), peaking at the pendant flower bud stage (Figure 8B). *MlRAD4* expression peaks in early flower development (Figure 8A). We found negligible expression of *MlRAD4* and *MlRAD5* in leaf and stem node tissue (Figure 8A, B).

We found a difference in expression patterns between the *MlRAD* paralogs across floral organs and between the dorsal/ventral regions of flowers. *MlRAD5* expression was high in 15 mm stage petals and carpels (Figure 8D), persisting just in carpels to the pendant stage (Figure 8D). *MlRAD4* expression was low to negligible across all floral organs at the 15 mm stage (Figure 8C) with increased expression just in sepals at the pendant stage (Figure 8C). We found that the relative expression of *MlRAD4* is not significantly different between the dorsal and ventral sides of flowers for any of the three developmental stages tested (5 mm, $P = 0.19$; 15 mm, $P = 0.46$; anthesis, $P = 0.48$; Figure 8E). We did find that expression of *MlRAD5* is significantly higher in dorsal tissues versus ventral tissues at the 5mm flower bud stage ($P = 0.0035$; Figure 8F). This pattern is consistent with *MlRAD5* contributing to dorsal flower differentiation similar to *A. majus RAD* (Corley et al., 2005). However, at the 15 mm and open flower stages we find similar *MlRAD5* relative expression levels in dorsal and ventral tissues, possibly due to relatively high but likely symmetric levels of *MlRAD5* expression in carpels at later stages of flower development (15 mm, $P = 0.88$; anthesis, $P = 0.67$; Figure 8F).

*MlCYC1*_RNAi and *MlCYC2*_RNAi lines are partially ventralized with stronger phenotypes in *MlCYC1*_RNAi lines

We generated 16 *MlCYC1* and 12 *MlCYC2* independent RNAi transgenic lines, confirmed by PCR screens for insertion of the transgene in gDNA (data not shown). Of these, we selected 4 *MlCYC1*_RNAi and 6 *MlCYC2*_RNAi lines for further expression and phenotypic analyses (*MlCYC1*_RNAi-13, 14, 15, 16; *MlCYC2*_RNAi-1, 3, 4, 5, 8, 11).

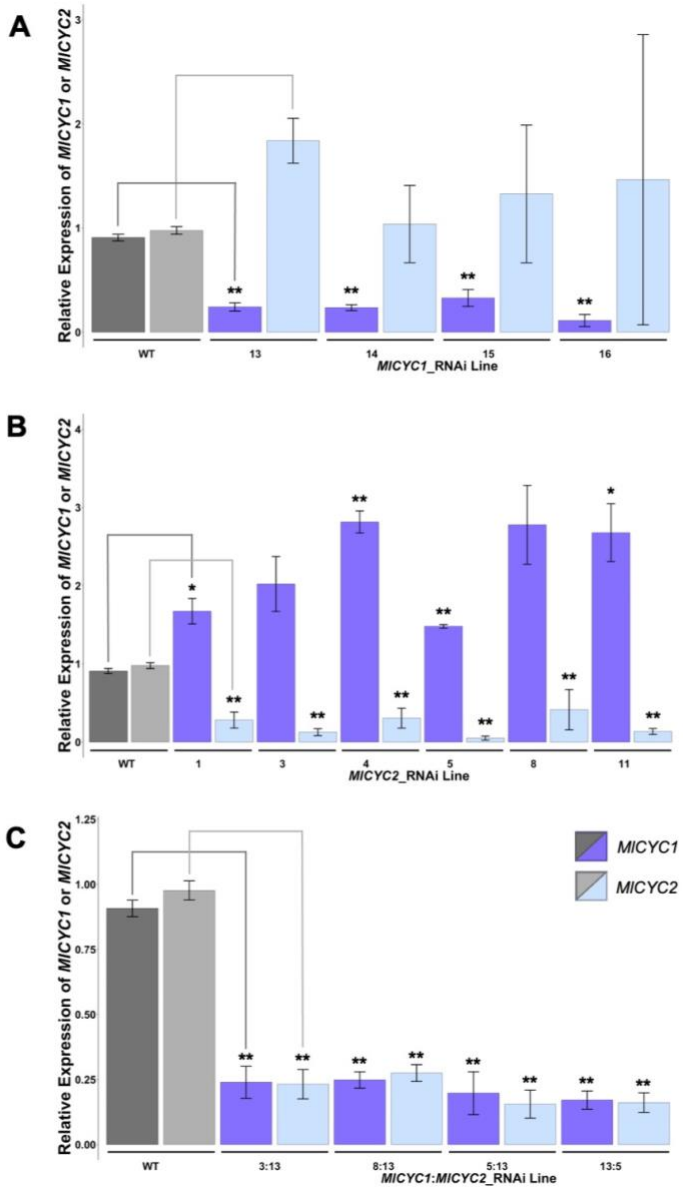

Figure 9. Relative expression of *MlCYC1* and *MlCYC2* in RNAi lines. (A) *MlCYC1* and *MlCYC2* expression in 4 *MlCYC1*_RNAi lines. (B) *MlCYC1* and *MlCYC2* expression in 6 *MlCYC2*_RNAi lines. (C) *MlCYC1* and *MlCYC2* expression in 4 *MlCYC1*:*MlCYC2*_RNAi lines. All expression data were collected from 15 mm stage flower buds. All relative expression is normalize to the wild-type. (T-test; *, 5% significance level; **, 1% significance level).

We confirmed *MlCYC1* and *MlCYC2* expression knockdown in *MlCYC1*_RNAi and *MlCYC2*_RNAi lines, respectively, by qRT-PCR. For all 10 independent RNAi lines, target gene expression levels were significantly reduced (*MlCYC1*_RNAi: *P* ranges from $2.2x10^{-5}$-0.00067; *MlCYC2*_RNAi: *P* ranges from $7.6x10^{-6}$-0.028; Figure 9A, B). Downregulation ranged from 64 to 88% in *MlCYC1*_RNAi lines and from 69 to 95% in *MlCYC2*_RNAi lines compared to *M. lewisii* LF10.

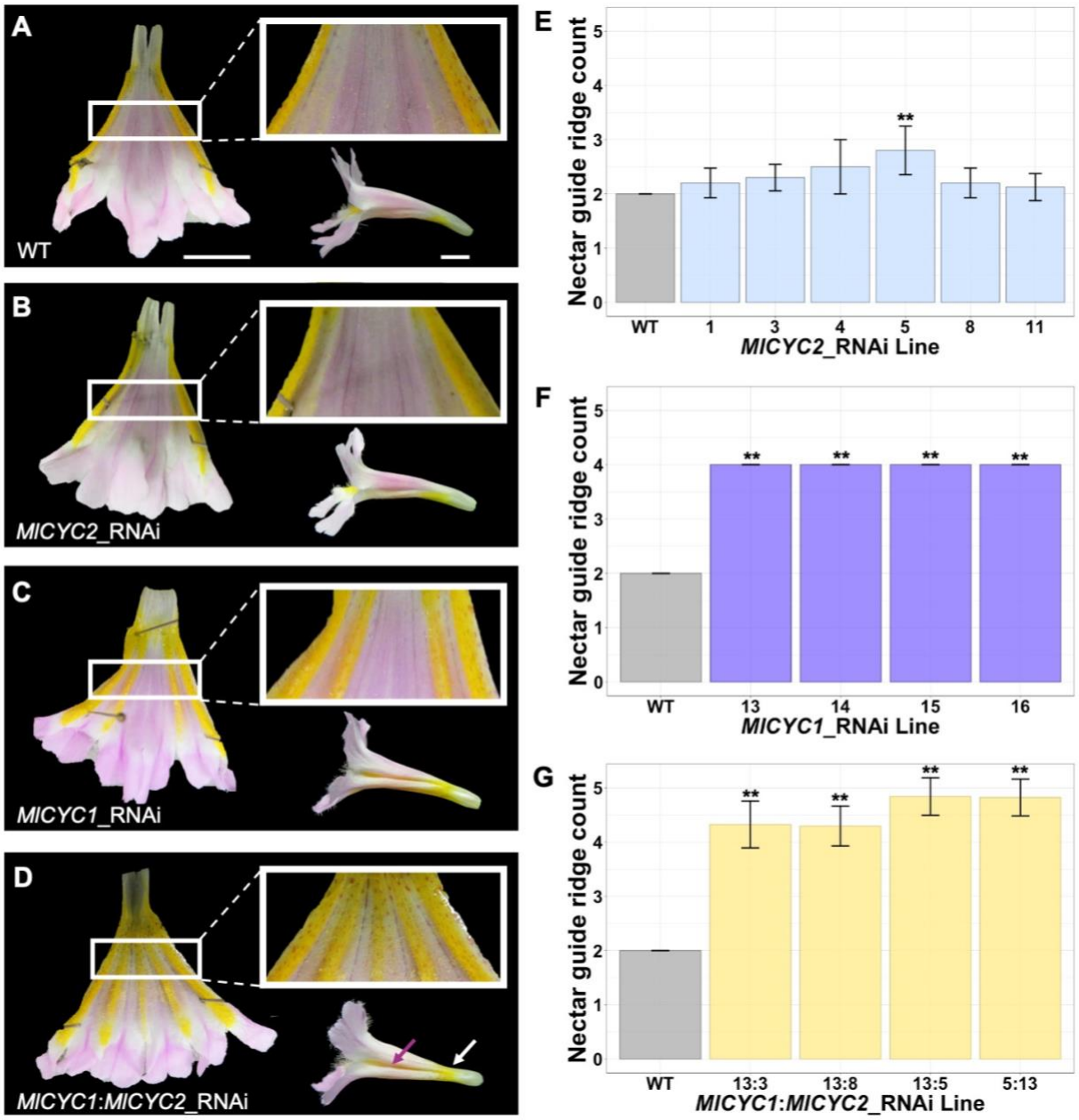

Figure 10. Characterization of nectar guide ridge count of RNAi lines compared to wild-type *M. lewisii*. Dissected corolla tubes exposing interior surface and side view of wild-type (A), *MlCYC2* (B), *MlCYC1* (C), and *MlCYC1*:*MlCYC2* (D) RNAi line flowers; (white arrow indicates constriction at base of corolla tube; pink arrow indicates in-pocketing of the nectar guide ridge); (scale bars, 1 cm). Counts of nectar guide ridges for *MlCYC2* (E), *MlCYC1* (F), *MlCYC1*:*MlCYC2* RNAi lines (G); (grey, wild-type; blue, *MlCYC2*_RNAi; purple, *MlCYC1*_RNAi; yellow, *MlCYC1*:*MlCYC2*_RNAi); (T-test; *, 5% significance level; **, 1% significance level).

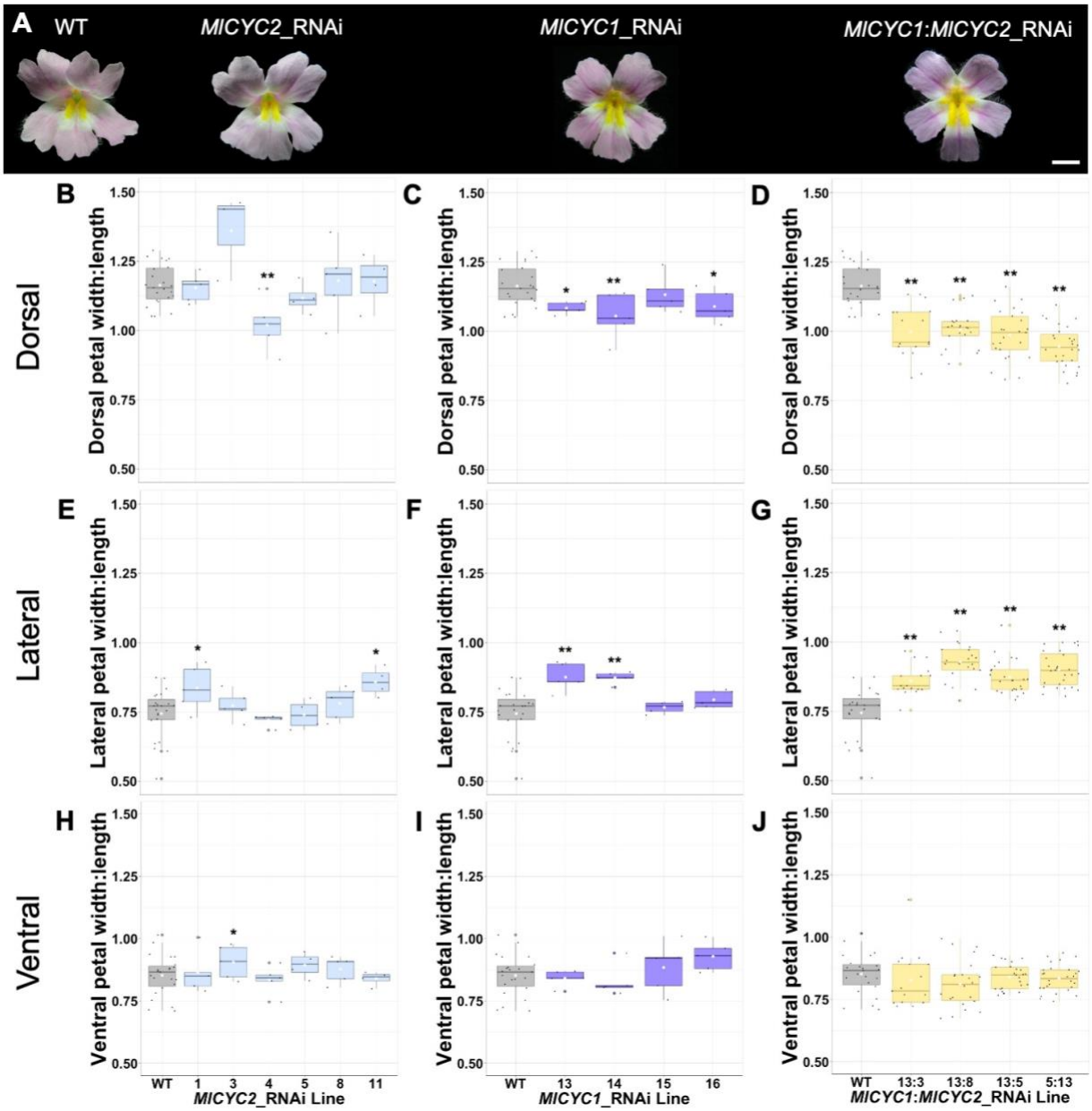

Figure 11. Characterization of petal shape of RNAi lines compared to wild-type *M. lewisii*. Face view of wild-type, *MlCYC2*, *MlCYC1*, and *MlCYC1*:*MlCYC2* RNAi line flowers (A), (scale bar, 1 cm). Boxplots of dorsal petal width:length ratios for *MlCYC2* (B), *MlCYC1* (C), *MlCYC1*:*MlCYC2* RNAi lines (C); lateral petal width:length ratios for *MlCYC2* (E), *MlCYC1* (F), *MlCYC1*:*MlCYC2* RNAi lines (G); ventral petal width:length ratios for *MlCYC2* (H), *MlCYC1* (I), *MlCYC1*:*MlCYC2* RNAi lines (J); (grey, wild-type; blue, *MlCYC2*_RNAi; purple, *MlCYC1*_RNAi; yellow, *MlCYC1*:*MlCYC2*_RNAi); (T-test; *, 5% significance level; **, 1% significance level).

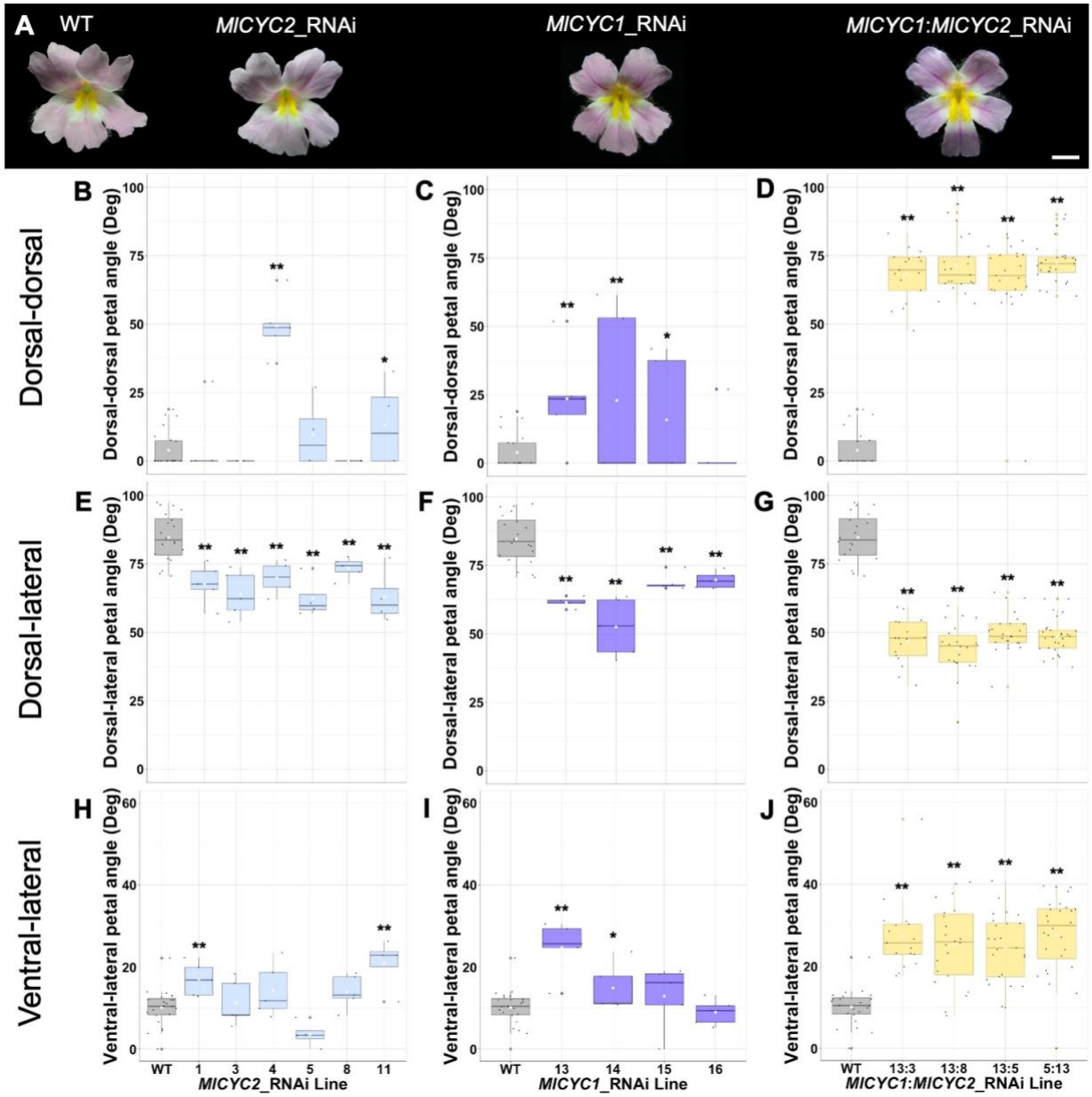

Figure 12. Characterization of the divergence angle between petals of RNAi lines compared to wild-type *M. lewisii*. Face view of wild-type, *MlCYC2*, *MlCYC1*, and *MlCYC1*:*MlCYC2* RNAi flowers (A), (scale bar, 1 cm). Boxplots of dorsal-dorsal petal angle for *MlCYC2* (B), *MlCYC1* (C), *MlCYC1*:*MlCYC2* RNAi lines (C); dorsal-lateral petal angle for *MlCYC2* (E), *MlCYC1* (F), *MlCYC1*:*MlCYC2* RNAi lines (G); ventral-lateral petal angle for *MlCYC2* (H), *MlCYC1* (I), *MlCYC1*:*MlCYC2* RNAi lines (J); (grey, wild-type; blue, *MlCYC2*_RNAi; purple, *MlCYC1*_RNAi; yellow, *MlCYC1*:*MlCYC2*_RNAi); (T-test; *, 5% significance level; **, 1% significance level).

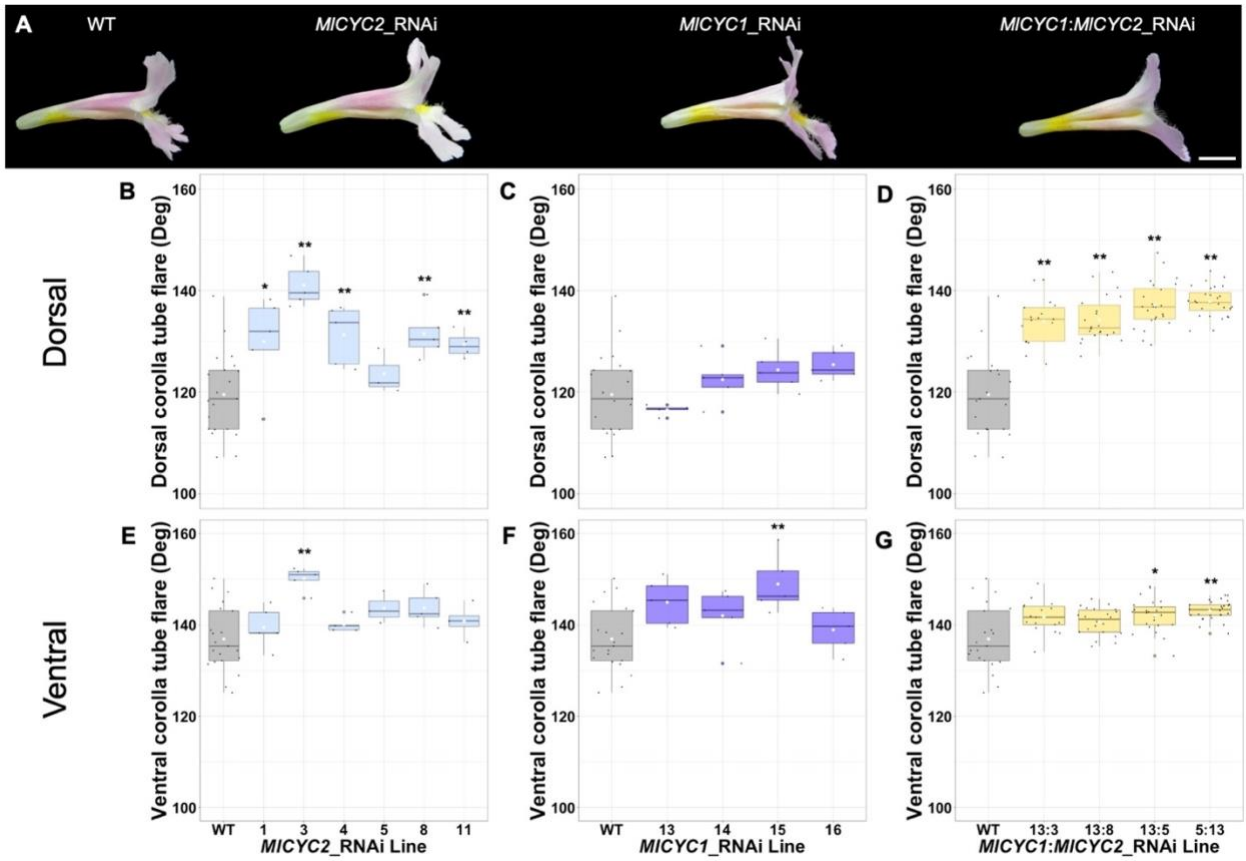

Figure 13. Characterization of the corolla tube flare of RNAi lines compared to wild-type *M. lewisii*. Side view of wild-type, *MlCYC2*, *MlCYC1*, and *MlCYC1*:*MlCYC2* RNAi flowers (A), (scale bar, 1 cm). Boxplots of dorsal corolla tube flare for *MlCYC2* (B), *MlCYC1* (C), *MlCYC1*:*MlCYC2* RNAi lines (C); ventral corolla tube flare for *MlCYC2* (E), *MlCYC1* (F), *MlCYC1*:*MlCYC2* RNAi lines (G); (grey, wild-type; blue, *MlCYC2*_RNAi; purple, *MlCYC1*_RNAi; yellow, *MlCYC1*:*MlCYC2*_RNAi); (T-test; *, 5% significance level; **, 1% significance level).

To test for changes in floral morphology we characterized flower phenotypes from *MlCYC1* and *MlCYC2* RNAi lines compared to *M. lewisii* LF10 wild-type. We focused on development of nectar guides, petal shape which was determined by taking the ratio of petal width to length to minimize variation resulting from plasticity in flower size, the divergence angles between petals, and the extent of corolla tube flare based on the angle of divergence between the dorsal and ventral petal lobes to tubes (Figures 10-13; Table A6). We found that both *MlCYC1*_RNAi lines and *MlCYC2*_RNAi lines exhibited floral phenotypes that trended towards ventralization of the flower, with stronger patterns of ventralization in *MlCYC1*_RNAi

lines. Qualitatively, we did not identify any vegetative differences between *MlCYC* RNAi lines and LF10 wild-type.

The most diagnostic trait for assessing ventralization was the number of nectar guide ridges (Figure 10). Wild-type *M. lewisii* LF10 flowers developed 2 nectar guide ridges on the ventral corolla (Figure 10A; Table A6). *MlCYC2*_RNAi lines showed some variation in this trait with a trend towards increased nectar guide ridge number, but rarely a significant difference from wild-type (*P* ranges from 0.016-0.39; Figure 10B, E; Table A6). All *MlCYC1*_RNAi lines showed significant increase in nectar guide ridge production with two additional nectar guides on lateral petals ($P = 6.0 \times 10^{-12}$ for all lines; Figure 10C, F; Table A6), a clear indication of ventralization of lateral flower identity in *MlCYC1*_RNAi lines.

In addition to nectar guide ridge differences, we found that *MlCYC1*_RNAi and *MlCYC2*_RNAi lines showed changes in petal dimensions, the angle between petals, and corolla tube flare that together indicated partial flower ventralization. In both *MlCYC1* and *MlCYC2* RNAi lines we saw a trend towards increased lateral petal width:length ratio (*MlCYC1*_RNAi: *P* ranges from 0.0039-0.59; *MlCYC2*_RNAi: *P* ranges from 0.021-0.93; Figure 11E, F; Table A6) and decreased dorsal petal width:length ratio (*MlCYC1*_RNAi: *P* ranges from 0.0067-0.39; *MlCYC2*_RNAi: *P* ranges from 0.00078-0.80; Figure 11B, C; Table A6). In both *MlCYC1* and *MlCYC2* RNAi lines we saw a trend towards increase in the angle between dorsal petals (*MlCYC1*_RNAi: *P* ranges from 0.00027-0.69; *MlCYC2*_RNAi: *P* ranges from 1.8×10^{-12}-0.63; Figure 12B, C; Table A6), decrease in the angle between dorsal and lateral petals (*MlCYC1*_RNAi: *P* ranges from 2.8×10^{-7}-0.00090; *MlCYC2*_RNAi: *P* ranges from 6.4×10^{-5}-0.0076; Figure 12E, F; Table A6), and increase in the angle between ventral and lateral petals (*MlCYC1*_RNAi: *P* ranges from 1.8×10^{-6}-0.60; *MlCYC2*_RNAi: *P* ranges from 0.00027-0.61;

Figure 12H, I; Table A6). In both *MlCYC1* and *MlCYC2* RNAi lines we saw a trend towards increase angle in the dorsal corolla tube flare (*MlCYC1*_RNAi: *P* ranges from 0.092-0.72; *MlCYC2*_RNAi: *P* ranges from $1.1x10^{-5}$-0.20; Figure 13B, C; Table A6), and increase angle in the ventral corolla tube flare (*MlCYC1*_RNAi: *P* ranges from 0.0091-0.85; *MlCYC2*_RNAi: *P* ranges from 0.0.0030-0.73; Figure 13E, F; Table A6). These trends bring lateral and dorsal petals closer to wild-type ventral petal dimensions.

***MlCYC1*:*MlCYC2* RNAi lines develop fully radialized flowers**

By cross-pollinating single *MlCYC1*_RNAi with *MlCYC2*_RNAi lines we generated double silenced *MlCYC1*:*MlCYC2* RNAi lines. We selected four independent crosses confirmed by PCR (data not shown) for expression analysis and phenotypic characterization. The parental contributions of these crosses include: line *MlCYC1*_RNAi-13 for all four crosses; three crosses have unique *MlCYC2* parents (*MlCYC2*_RNAi-3, *MlCYC2*_RNAi-5, *MlCYC2*_RNAi-8); and two of these crosses are reciprocals (*MlCYC1*_RNAi-13:*MlCYC2*_RNAi-5, *MlCYC2*_RNAi-5:*MlCYC1*_RNAi-13). We determined knockdown of *MlCYC1* and *MlCYC2* in double RNAi lines by performing qRT-PCR. We found transcript levels of *MlCYC1* and *MlCYC2* in *MlCYC1*:*MlCYC2*_RNAi lines were significantly downregulated by 75 to 83% and 73 to 85%, respectively, compared to wild-type (*P* ranged from $1.3x10^{-6}$-0.00014 for *MlCYC1* and $1.2x10^{-6}$-$8.3x10^{-5}$ for *MlCYC2* across all lines; Figure 9C).

Across *MlCYC1:MlCYC2*_RNAi lines, we found flowers to be nearly or fully radialized through expansion of ventral identity into the lateral and dorsal regions of the flower. Qualitatively, we did not identify any vegetative differences between these double lines and LF10 wild-type. As with the single RNAi lines, nectar guide ridges provided the clearest indication of ventralization. In all *MlCYC1*:*MlCYC2*_RNAi lines we observed a significant gain

of 2 to 3 additional nectar guide ridges (*P* ranging from $5.6x10^{-39}$-$8.4x10^{-26}$; Figure 10D, G; Table A6); flowers with 5 nectar guide ridges were fully radialized. These additional nectar guide ridges developed between the dorsal and lateral petals as well as between the two dorsal petals. In fully-formed nectar guide ridges, we observed carotenoid pigment with anthocyanin pigment spots and increased trichome density. Formation of nectar guide ridges were additionally visible from the outside of the flower as in-pocketings along the corolla tube (Figure 10D).

In addition to nectar guide ridge differences, we found that *MlCYC1:MlCYC2* RNAi lines showed changes in petal dimensions, the angle between petals, and corolla tube flare consistent with complete or nearly complete ventralization of flowers. In all double RNAi lines compared to wild-type, we found significantly smaller width:length ratio for dorsal petals (*P* ranged from $2.1x10^{-14}$-$2.5x10^{-7}$; Figure 11D; Table A6), significantly larger width:length ratio for lateral petals (*P* ranges from $7.4x10^{-10}$-$3.1x10^{-5}$; Figure 11G; Table A6), and no change to ventral petal shape (*P* ranges from 0.13-0.53; Figure 11J; Table A6). In all double RNAi lines compared to wild-type, the angle between dorsal petals and the ventral-lateral petals increased significantly (dorsal-dorsal: *P* ranges from $3.9x10^{-36}$-$2.5x10^{-25}$, and ventral-lateral: *P* ranges from $7.1x10^{-11}$-$3.0x10^{-8}$ across lines; Figure 12D, J; Table A6), while the angle between dorsal and lateral petals decreased significantly (*P* ranges from $1.2x10^{-21}$-$4.9x10^{-16}$ across lines; Figure 12G; Table A6).

In double RNAi lines compared to wild-type, we found the dorsal and ventral corolla tube flare significantly increased in angle, resulting in a decrease in flare for both regions (dorsal: *P* ranges from $1.9x10^{-14}$-$9.8x10^{-8}$ all lines; ventral: *P* ranges from 0.0026-0.17 most lines; Figure 13D, G; Table A6). In addition, the corolla tube in double lines was straight compared to wild-

type, with a pronounced constriction at the base of the corolla tube accompanied by increased carotenoid pigment (Figure 10D).

MlRAD5 is downregulated in both petals and carpels of the *MlCYC1*:*MlCYC2* RNAi Background.

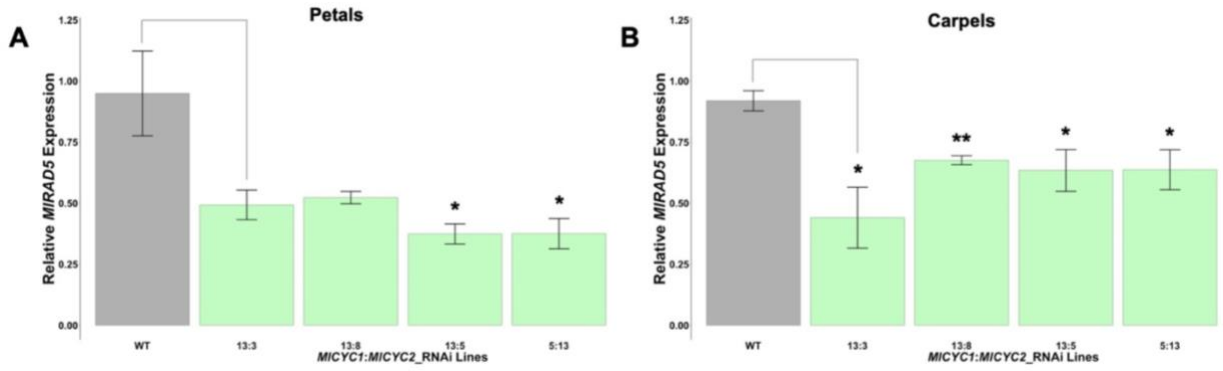

Figure 14. Relative expression of *MlRAD5* in *MlCYC1*:*MlCYC2* RNAi lines. (A) *MlRAD5* expression in petal+attached stamens in 4 *MlCYC1*:*MlCYC2*_RNAi lines. (B) *MlRAD5* expression in carpels in 4 *MlCYC-1*:*MlCYC2*_RNAi lines. All expression data were collected from 15 mm stage flower buds. All relative expression is normalize to the wild-type. (T-test; *, 5% significance level; **, 1% significance level).

To determine if *MlCYC1* and/or *MlCYC2* positively regulate *MlRAD5*, similar to *AmCYC/AmDICH* positive regulation of *AmRAD*, we performed qRT-PCR to quantify transcript levels of *MlRAD5* in floral tissues of *MlCYC1*:*MlCYC2*_RNAi lines. We found that *MlRAD5* was marginally to significantly downregulated in both petal+stamen and gynoecium tissues, by 45 to 61% and 27 to 52%, respectively (petal+stamen tissues: *P* ranges from 0.032-0.072; gynoecium tissue: *P* ranges from 0.0055-0.039; Figure 14).

DISCUSSION

Expression of *MlCYC1*, *MlCYC2* and *MlRAD5* is consistent with roles in both dorsal perianth and carpel development

In *M. lewisii*, the expression of *MlCYC1* and *MlCYC2* was present in whole flower buds from early to late flower development stages with strong and specific expression in dorsal

perianth tissue (Figure 7). This is similar to *CYC* expression in other Lamiales, including other species of *Mimulus,* with bilateral flower symmetry (Luo et al., 1996, 1999; Zhong et al., 2017; Zhong & Kellogg, 2015b). This overall pattern of dorsal-specific perianth expression supports the conclusion that these genes, after duplication, are conserved in patterning bilateral flower symmetry in *M. lewisii*.

Both *MlRAD4* and *MlRAD5* are closely related to the dorsal flower identity gene, *RAD* in *A. majus* (Sengupta & Hileman, 2018). Whether one or both play a role in *M. lewisii* dorsal flower development is an open question. Here, we found that *MlRAD5,* but not *MlRAD4* (Figure 8) has dorsal-specific perianth expression, similar to *A. majus*, where *AmRAD* expression is restricted to the dorsal region of developing flowers (Corley et al., 2005). This provides strong evidence that only *MlRAD5* retained the flower symmetry developmental function following the duplication that led to *MlRAD4* and *MlRAD5* paralogous gene lineages.

In addition to these expected patterns of dorsal-specific *CYC* and *RAD* expression in *M. lewisii,* we found high expression in carpels for *MlCYC1* (the *CYC2B* paralog; Figure 7C) and *MlRAD5* (Figure 8D). This pattern of *CYC2B* lineage and *RAD5* lineage gene expression was previously identified in *M. guttatus* (Zhong et al., 2017), but little was made of the pattern. Our findings, coupled with those of Zhong *et al.* (2017) suggest that the *CYC-RAD* regulatory module may have an additional function outside of establishing perianth symmetry. Specifically, this module may function in a previously un-identified aspect of carpel and/or ovule development as hypothesized by Sengupta and Hileman (in review).

MlCYC1 and *MlCYC2* function redundantly to regulate dorsal flower identity in *M. lewisii*

Using an RNAi stable transformation approach, we found that *MlCYC1* and *MlCYC2* exhibit extensive, but not fully redundant functions in establishing dorsal flower identity (Figures

10-13). *MlCYC1* can completely compensate for loss of *MlCYC2* function. *MlCYC2*_RNAi lines are, nearly always, not significantly different from wild-type in aspects of petal and stamen development. On the other hand, *MlCYC2* cannot completely compensate for loss of *MlCYC1* function. *MlCYC1*_RNAi lines are nearly always significantly different from wild-type in aspects of petal and stamen development. These lines exhibit a trend towards flower ventralization, for example, an increase to four nectar guide ridges (Figure 10C, F; Table A6). It is unlikely that lack of phenotype in *MlCYC2*_RNAi lines is due to lack of endogenous *MlCYC2* downregulation. *MlCYC2* expression is similarly downregulated in *MlCYC2*_RNAi lines as *MlCYC1* is in *MlCYC1*_RNAi lines (Figure 9A, B), and these levels of downregulation are also comparable to previous RNAi knockdown experiments in *M. lewisii* LF10 (LaFountain et al., 2017; Yuan, Sagawa, Young, et al., 2013).

This pattern of paralog redundancy is similar to *CYC* and *DICH* redundancy in *A. majus* where *CYC* can largely compensate for loss of *DICH* function, but *DICH* cannot compensate for loss of *CYC* function (Luo et al., 1996, 1999). However, in *A. majus* the *DICH* paralog has clearly evolved a novel function in specifying the internal asymmetry of dorsal petals in addition to retaining partial function of specifying dorsal flower identity (Luo et al., 1999). Our characterization of individual *MlCYC1*_RNAi and *MlCYC2*_RNAi lines did not provide evidence of any clear novel roles for either *MlCYC1* or *MlCYC2*. This includes no clear defects in carpel development despite strong expression of *MlCYC1* in carpels. We did not fully characterize all aspects of carpel development (*e.g.*, carpel wall width, septum patterning), nor did we fully characterize ovule phenotypes. If carpel or ovule development is disrupted in *MlCYC1*_RNAi lines (or *MlCYC1:MlCYC2*_RNAi lines), it will require further detailed characterization to uncover.

Together, *MlCYC1* and *MlCYC2* are sufficient to specify dorsal *M. lewisii* flower development. *MlCYC1*:*MlCYC2*_RNAi flowers revealed a radialized phenotype compared to *M. lewisii* LF10 flowers. In double lines, we identified changes in dorsal and lateral petals that strongly trended towards ventral characteristics, including the addition of extra nectar guide ridges and changes in petal shape. In all *MlCYC1*:*MlCYC2* RNAi lines there was a gain of two to three additional nectar guide ridges found in the dorsal and lateral corolla tube (Figure D, G). In these lines, dorsal petals narrowed and lateral petals widened. The average dorsal and lateral petal width:length ratios were within the range of that of the wild-type ventral petals (Table A6). We found that as double lines trended towards radialization, all angles between petal lobes converged towards similar and often overlapping values, with the dorsal-dorsal petal angle and ventral-lateral petal angles widened, and dorsal-lateral petal angles narrowed. This is expected in radialized flowers as equal angles between all petals is a characteristic of naturally radially symmetric flowers. Changes to the corolla tube flare of the dorsal region trended towards that of the ventral region as well (Figure 13A, D), with an increased angle such that the dorsal petals reduced their banner petal appearance.

Wild-type *M. lewisii* flowers have four fertile stamens and no stamen in the dorsal position of the flower (highly reduced so as not to be evident, but presumed aborted during flower development). We observed a gain of one additional stamen in the dorsal position across multiple *MlCYC1*:*MlCYC2*_RNAi plants, increasing the whorl from four to five fertile stamens. Therefore, similar to *A. majus*, the dorsal identity *CYC* genes control both corolla and androecium dorsal identity in *M. lewisii.* However, the gain of one stamen was not consistent in any one line. Unlike in *A. majus cyc:dich* double mutants where flowers often increase from five to six organs per whorl (Luo et al., 1999), we did not find any changes to overall merosity in

MlCYC1:*MlCYC2*_RNAi flowers. Sepal, petal and stamen whorls consistently developed five organs with a bi-carpelate ovule. In *M. guttatus* VIGS experiments, increases in petal and stamen merosity were reported in double *MgCYC1*:*MgCYC2* silenced lines, though highly variable (Preston et al., 2014). In these same *MgCYC1*:*MgCYC2* silenced lines, there were reported instances of one additional carpel (Preston et al., 2014). Given the rarity of these phenotypes in the VIGS experiments, it is not clear that suppression of both *MgCYC1* and *MgCYC2* paralogs in *M. guttatus* consistently leads to changes in merosity similar to *A. majus.* Determining whether *CYC* genes uniquely control merosity in *A. majus*, or more broadly control merosity with loss of this function in *M. lewisii*, requires more detailed functional studies using stable transformation or mutagenic studies which provide consistent loss-of-function phenotypes, both in *M. guttatus* and in other HCL.

MlCYC1 and/or *MlCYC2* regulate *MlRAD5*

In *A. majus*, the expression pattern of *AmRAD* mirrors that of *AmCYC* and, to some extent, *AmDICH*, beginning at 'flower stage two', just after initiation of *AmCYC* and *AmDICH* expression (Corley et al., 2005). Also, *AmRAD* expression is not observed in the *cyc*:*dich* mutant and the *rad* mutant has a near-complete radialized floral phenotype, approaching the *cyc*:*dich* mutant phenotype (Corley et al., 2005). These lines of evidence, along with the identification of multiple conserved TCP binding sites in the putative *RAD* promoter (Sengupta & Hileman, 2018), strongly suggest that *AmCYC* and *AmDICH* are direct activators of *AmRAD* (Corley et al., 2005). Our data suggest that *MlCYC1* and/or *MlCYC2* positively regulate *MlRAD5* during *M. lewisii* flower development. In our *MlCYC1*:*MlCYC2*_RNAi lines we found downregulation of *MlRAD5* in both carpel and petal tissues, where both floral organs had high *MlRAD5* expression

in wild-type (Figure 14). Further research is required to verify the influence of *MlCYC1* versus *MlCYC2* in the positive regulation of *MlRAD5* during both petal and carpel development.

Both *MlCYC1* and *MlCYC2* are retained following an ancient duplication event

MlCYC1 and *MlCYC2* belonging to the HCL ECE-*CYC2B* and ECE-*CYC2A* gene lineages, respectively. Therefore, these paralogs derive from a relatively ancient duplication event which occurred before the radiation of the HCL, between 40.1-71.3 Mya (Zhong & Kellogg, 2015b). Yet both paralogs persist. Duplicated genes are proposed to have one of three primary fates (Force et al., 1999; Ganko et al., 2007; Lynch & Force, 2000): 1) neofunctionalization, one paralog evolves a novel function, while the other retains the ancestral function; 2) subfunctionalization, paralogs partition the ancestral function or 3) nonfunctionalization, one paralog accumulates deleterious mutations that lead to pseudogene formation. While pseudogene formation is expected to be the most likely outcome (Force et al., 1999; Lynch & Force, 2000), in plant genomes we find large numbers of paralogs are retained (Panchy et al., 2016). Studies suggest that the fate of duplicated genes depends on the mechanism of duplication (*e.g.* whole genome duplication or small-scale duplication) (Rensing, 2014), as well as selective constraints (Mondragón-Palomino & Theißen, 2009) and the influence of molecular and biological functions (Hanada et al., 2008; Maere et al., 2005). Here, we can just begin to speculate on the mechanisms underlying maintenance of both *MlCYC1* and *MlCYC2* paralogs.

MlCYC1 is selectively retained, at least in part, due its role in establishing dorsal flower identity. Loss of *MlCYC1* function in *MlCYC1*_RNAi lines leads to subtle changes in flower shape. Specifically, slight expansion of ventral identity into lateral regions of the flower. We hypothesize that naturally occurring variants for loss of *MlCYC1* function would have reduced

fitness due to reduced pollinator visitation or inefficient pollen transfer. While *MlCYC1*_RNAi lines were able to undergo seed set and fruit development following self- and cross-fertilization, it is also possible that the high levels of *MlCYC1,* and downstream *MlRAD5* expression that we observed in *M. lewisii* carpels is associated with a specific and as yet unidentified function for these genes in fruit, ovule or seed development. Therefore, there could be appreciable fitness consequences due to carpel, ovule or seed developmental defects in naturally occurring loss of *MlCYC1* variants.

On the other hand, we did not see observable defects in flower development across multiple *MlCYC2*_RNAi lines. Therefore, natural variants defective in *MlCYC2* function should presumably have similar fitness to wild-type, and *MlCYC2* loss-of-function mutations could drift to fixation. That this has not occurred suggests that *MlCYC2* is selectively maintained for reasons we have not identified. It is possible that residual expression of *MlCYC2* in *MlCYC2*_RNAi lines is sufficient for *MlCYC2* function and therefore we are not capturing true loss-of-function phenotypes. This is unlikely given that *MlCYC2* downregulation in *MlCYC2*_RNAi lines is similar to *MlCYC1* downregulation in *MlCYC1*_RNAi lines (Figure 9A, B). More likely is that there are fitness effects for loss of *MlCYC2* that we have not captured in this study. This is different from the situation in *A. majus* where *DICH,* which does function redundantly with *CYC* to establish dorsal flower identity, has clearly adopted a novel function in specifying the internal shape of the dorsal petals (Luo et al., 1999). It is possible that the only way to confirm *MlCYC2* loss-of-function fitness effects would be through field experiments comparing fitness of *MlCYC2*_RNAi lines to wild-type. This is because it is not clear what the expected phenotypic effects to loss of *MlCYC2* function might be given our current understanding of *MlCYC2* spatial and temporal patterns of expression.

CONCLUSION

Bilateral flower symmetry is an adaptive flower trait that has evolved independently numerous times across the angiosperm phylogeny. The ECE-*CYC2* gene lineage has been repeatedly recruited in the genetic control of bilateral flower symmetry development. Additionally, the ECE-*CYC2* gene lineage has undergone extensive duplications, with many duplication events linked to transitions in flower symmetry. In this study we tested for conservation of the bilateral flower symmetry developmental program between *A. majus* and *M. lewisii*, where both genomes contain independent duplications of the ECE-*CYC2* gene lineage. We demonstrate the expression and function of *MlCYC* and *MlRAD* genes are similar to those previously determined for *A. majus CYC*, *DICH*, and *RAD—MlCYC* paralogs show a high degree of functional redundancy in patterning dorsal flower development, and these genes positively regulate *MlRAD5* similar to the program in *A. majus.* However, maintenance of *MlCYC2* is less clear since we found no evidence for novel function of this gene in addition to its apparent complete redundancy with *MlCYC1* in establishing dorsal flower identity. Unique to *Mimulus* is the strong expression of *MlCYC1* and *MlRAD5* during early carpel development. Future studies should focus on determining the function of these canonical symmetry genes in carpel, ovule and/or seed development.

References

Almeida, J., Rocheta, M., & Galego, L. (1997). Genetic control of flower shape in Antirrhinum majus. *Development*, *124*, 1387–1392.

Bartlett, M. E., & Specht, C. D. (2011). Changes in expression pattern of the teosinte branched1-like genes in the Zingiberales provide a mechanism for evolutionary shifts in symmetry across the order. *American Journal of Botany*, *98*(2), 227–243. https://doi.org/10.3732/ajb.1000246

Bergbusch, V. (1999). A Note on the Manipulation of Flower Symmetry inAntirrhinum majus. *Annals of Botany*, *83*(5), 483–488. https://doi.org/10.1006/anbo.1998.0844

Broholm, S. K., Tähtiharju, S., Laitinen, R. A. E., Albert, V. A., Teeri, T. H., & Elomaa, P. (2008). A TCP domain transcription factor controls flower type specification along the radial axis of the *Gerbera* (Asteraceae) inflorescence. *Proceedings of the National Academy of Sciences*, *105*(26), 9117–9122. https://doi.org/10.1073/pnas.0801359105

Busch, A., Horn, S., Muhlhausen, A., Mummenhoff, K., & Zachgo, S. (2012). Corolla Monosymmetry: Evolution of a Morphological Novelty in the Brassicaceae Family. *Molecular Biology and Evolution*, *29*(4), 1241–1254. https://doi.org/10.1093/molbev/msr297

Busch, A., & Zachgo, S. (2007). Control of corolla monosymmetry in the Brassicaceae Iberis amara. *Proceedings of the National Academy of Sciences*, *104*(42), 16714–16719. https://doi.org/10.1073/pnas.0705338104

Chapman, M. A., Leebens-Mack, J. H., & Burke, J. M. (2008). Positive Selection and Expression Divergence Following Gene Duplication in the Sunflower CYCLOIDEA Gene Family. *Molecular Biology and Evolution*, *25*(7), 1260–1273. https://doi.org/10.1093/molbev/msn001

Citerne, H. L., Le Guilloux, M., Sannier, J., Nadot, S., & Damerval, C. (2013). Combining Phylogenetic and Syntenic Analyses for Understanding the Evolution of TCP ECE Genes in Eudicots. *PLoS ONE*, *8*(9), e74803. https://doi.org/10.1371/journal.pone.0074803

Citerne, H. L., Luo, D., Pennington, R. T., Coen, E., & Cronk, Q. C. B. (2003). A Phylogenomic Investigation of CYCLOIDEA-Like TCP Genes in the Leguminosae. *Plant Physiology*, *131*(3), 1042–1053. https://doi.org/10.1104/pp.102.016311

Citerne, H. L., Reyes, E., Le Guilloux, M., Delannoy, E., Simonnet, F., Sauquet, H., Weston, P. H., Nadot, S., & Damerval, C. (2017). Characterization of CYCLOIDEA-like genes in Proteaceae, a basal eudicot family with multiple shifts in floral symmetry. *Annals of Botany*, *119*(3), 367–378. https://doi.org/10.1093/aob/mcw219

Citerne, H., Pennington, R. T., & Cronk, Q. C. B. (2006). An apparent reversal in floral symmetry in the legume Cadia is a homeotic transformation. *Proceedings of the National Academy of Sciences*, *103*(32), 12017–12020. https://doi.org/10.1073/pnas.0600986103

Corley, S. B., Carpenter, R., Copsey, L., & Coen, E. (2005). Floral asymmetry involves an interplay between TCP and MYB transcription factors in Antirrhinum. *Proceedings of the National Academy of Sciences of the United States of America*, *102*(14), 5068–5073. https://doi.org/10.1073/pnas.0501340102

Cubas, P., Lauter, N., Doebley, J., & Coen, E. (1999). The TCP domain: A motif found in proteins regulating plant growth and development. *The Plant Journal*, *18*(2), 215–222. https://doi.org/10.1046/j.1365-313X.1999.00444.x

Dellinger, A. S. (2020). Pollination syndromes in the 21st century: Where do we stand and where may we go? *New Phytologist*, *228*(4), 1193–1213. https://doi.org/10.1111/nph.16793

Dilcher, D. (2000). Toward a new synthesis: Major evolutionary trends in the angiosperm fossil record. *Proceedings of the National Academy of Sciences*, *97*(13), 7030–7036. https://doi.org/10.1073/pnas.97.13.7030

Ding, B., & Yuan, Y. (2016). Testing the utility of fluorescent proteins in Mimulus lewisii by an Agrobacterium-mediated transient assay. *Plant Cell Reports*, *35*(4), 771–777. https://doi.org/10.1007/s00299-015-1919-1

Doebley, J., Stec, A., & Hubbard, L. (1997). The evolution of apical dominance in maize. *Nature*, *386*(6624), 485–488. https://doi.org/10.1038/386485a0

Donoghue, M. J., Ree, R. H., & Baum, D. A. (1998). Phylogeny and the evolution of flower symmetry in the Asteridae. *Trends in Plant Science*, *3*(8), 1360–1385. https://doi.org/10.1016/S1360-1385(98)01278-3

Doyle, J. J., & Doyle, J. L. (1987). A rapid DNA isolation procedure for small quantities of fresh leaf tissue. *Phytochemical Bulletin*, *19*(1), 11–15.

Endress, P. K. (1994). *Diversity and evolutionary biology of tropical flowers*. Cambridge University Press.

Endress, P. K. (1999). Symmetry in Flowers: Diversity and Evolution. *International Journal of Plant Sciences*, *160*(S6), S3–S23. https://doi.org/10.1086/314211

Endress, P. K. (2001). Origins of flower morphology. *Journal of Experimental Zoology*, *291*(2), 105–115. https://doi.org/10.1002/jez.1063

Endress, P. K. (2012). The Immense Diversity of Floral Monosymmetry and Asymmetry Across Angiosperms. *The Botanical Review*, *78*(4), 345–397. https://doi.org/10.1007/s12229-012-9106-3

Feng, X., Zhao, Z., Tian, Z., Xu, S., Luo, Y., Cai, Z., Wang, Y., Yang, J., Wang, Z., Weng, L., Chen, J., Zheng, L., Guo, X., Luo, J., Sato, S., Tabata, S., Ma, W., Cao, X., Hu, X., … Luo, D. (2006). Control of petal shape and floral zygomorphy in Lotus japonicus. *Proceedings of the National Academy of Sciences*, *103*(13), 4970–4975. https://doi.org/10.1073/pnas.0600681103

Fenster, C. B., Armbruster, W. S., Wilson, P., Dudash, M. R., & Thomson, J. D. (2004). Pollination Syndromes and Floral Specialization. *Annual Review of Ecology, Evolution, and Systematics*, *35*(1), 375–403. https://doi.org/10.1146/annurev.ecolsys.34.011802.132347

Fernández-Mazuecos, M., Blanco-Pastor, J. L., Juan, A., Carnicero, P., Forrest, A., Alarcón, M., Vargas, P., & Glover, B. J. (2019). Macroevolutionary dynamics of nectar spurs, a key evolutionary innovation. *New Phytologist*, *222*(2), 1123–1138. https://doi.org/10.1111/nph.15654

Flagel, L. E., & Wendel, J. F. (2009). Gene duplication and evolutionary novelty in plants. *New Phytologist*, *183*(3), 557–564. https://doi.org/10.1111/j.1469-8137.2009.02923.x

Force, A., Lynch, M., Pickett, F. B., Amores, A., Yan, Y. L., & Postlethwait, J. (1999). Preservation of duplicate genes by complementary, degenerative mutations. *Genetics*, *151*(4), 1531–1545.

Friedman, W. E. (2009). The meaning of Darwin's "abominable mystery." *American Journal of Botany*, *96*(1), 5–21. https://doi.org/10.3732/ajb.0800150

Galego, L., & Almeida, J. (2002). Role of DIVARICATA in the control of dorsoventral asymmetry in Antirrhinum flowers. *Genes & Development*, *16*(7), 880–891. https://doi.org/10.1101/gad.221002

Ganko, E. W., Meyers, B. C., & Vision, T. J. (2007). Divergence in Expression between Duplicated Genes in Arabidopsis. *Molecular Biology and Evolution*, *24*(10), 2298–2309. https://doi.org/10.1093/molbev/msm158

Garcês, H. M. P., Spencer, V. M. R., & Kim, M. (2016). Control of Floret Symmetry by *RAY3, SvDIV1B* , and *SvRAD* in the Capitulum of *Senecio vulgaris*. *Plant Physiology*, *171*(3), 2055–2068. https://doi.org/10.1104/pp.16.00395

Gómez, J. M., Perfectti, F., & Camacho, J. P. M. (2006). Natural Selection on *Erysimum mediohispanicum* Flower Shape: Insights into the Evolution of Zygomorphy. *The American Naturalist*, *168*(4), 531–545. https://doi.org/10.1086/507048

Gubitz, T., Caldwell, A., & Hudson, A. (2003). Rapid Molecular Evolution of CYCLOIDEA-like Genes in Antirrhinum and Its Relatives. *Molecular Biology and Evolution*, *20*(9), 1537–1544. https://doi.org/10.1093/molbev/msg166

Hanada, K., Zou, C., Lehti-Shiu, M. D., Shinozaki, K., & Shiu, S.-H. (2008). Importance of Lineage-Specific Expansion of Plant Tandem Duplicates in the Adaptive Response to Environmental Stimuli. *Plant Physiology*, *148*(2), 993–1003. https://doi.org/10.1104/pp.108.122457

Herrera, J. (2009). Visibility vs. biomass in flowers: Exploring corolla allocation in Mediterranean entomophilous plants. *Annals of Botany*, *103*(7), 1119–1127. https://doi.org/10.1093/aob/mcp046

Hervé, C., Dabos, P., Bardet, C., Jauneau, A., Auriac, M. C., Ramboer, A., Lacout, F., & Tremousaygue, D. (2009). In Vivo Interference with AtTCP20 Function Induces Severe Plant Growth Alterations and Deregulates the Expression of Many Genes Important for

Development. *Plant Physiology*, *149*(3), 1462–1477. https://doi.org/10.1104/pp.108.126136

Hileman, L. C. (2014). Trends in flower symmetry evolution revealed through phylogenetic and developmental genetic advances. *Philosophical Transactions of the Royal Society B: Biological Sciences*, *369*(1648), 20130348. https://doi.org/10.1098/rstb.2013.0348

Hileman, L. C., & Baum, D. A. (2003). Why Do Paralogs Persist? Molecular Evolution of CYCLOIDEA and Related Floral Symmetry Genes in Antirrhineae (Veronicaceae). *Molecular Biology and Evolution*, *20*(4), 591–600. https://doi.org/10.1093/molbev/msg063

Hileman, L. C., Kramer, E. M., & Baum, D. A. (2003). Differential regulation of symmetry genes and the evolution of floral morphologies. *PNAS*, *100*(22), 12814–12819. https://doi.org/www.pnas.org cgi doi 10.1073 pnas.1835725100

Howarth, D. G., & Donoghue, M. J. (2005). Duplications in *CYC* -like Genes from Dipsacales Correlate with Floral Form. *International Journal of Plant Sciences*, *166*(3), 357–370. https://doi.org/10.1086/428634

Howarth, D. G., & Donoghue, M. J. (2006). Phylogenetic analysis of the "ECE" (CYC/TB1) clade reveals duplications predating the core eudicots. *Proceedings of the National Academy of Sciences*, *103*(24), 9101–9106. https://doi.org/10.1073/pnas.0602827103

Howarth, D. G., Martins, T., Chimney, E., & Donoghue, M. J. (2011). Diversification of CYCLOIDEA expression in the evolution of bilateral flower symmetry in Caprifoliaceae and Lonicera (Dipsacales). *Annals of Botany*, *107*(9), 1521–1532. https://doi.org/10.1093/aob/mcr049

Hsin, K.-T., Lu, J.-Y., Möller, M., & Wang, C.-N. (2019). Gene duplication and relaxation from selective constraints of GCYC genes correlated with various floral symmetry patterns in Asiatic Gesneriaceae tribe Trichosporeae. *PLOS ONE*, *14*(1), e0210054. https://doi.org/10.1371/journal.pone.0210054

Hsin, K.-T., & Wang, C.-N. (2018). Expression shifts of floral symmetry genes correlate to flower actinomorphy in East Asia endemic Conandron ramondioides (Gesneriaceae). *Botanical Studies*, *59*, 24. https://doi.org/10.1186/s40529-018-0242-x

Jabbour, F., Cossard, G., Le Guilloux, M., Sannier, J., Nadot, S., & Damerval, C. (2014). Specific Duplication and Dorsoventrally Asymmetric Expression Patterns of Cycloidea-Like Genes in Zygomorphic Species of Ranunculaceae. *PLoS ONE*, *9*(4), e95727. https://doi.org/10.1371/journal.pone.0095727

Juntheikki-Palovaara, I., Tähtiharju, S., Lan, T., Broholm, S. K., Rijpkema, A. S., Ruonala, R., Kale, L., Albert, V. A., Teeri, T. H., & Elomaa, P. (2014). Functional diversification of duplicated CYC2 clade genes in regulation of inflorescence development in Gerbera hybrida (Asteraceae). *The Plant Journal*, *79*(5), 783–796. https://doi.org/10.1111/tpj.12583

Kerschen, A., Napoli, C. A., Jorgensen, R. A., & Müller, A. E. (2004). Effectiveness of RNA interference in transgenic plants. *FEBS Letters*, *566*(1–3), 223–228. https://doi.org/10.1016/j.febslet.2004.04.043

Kosugi, S., & Ohashi, Y. (1997). PCF1 and PCF2 specifically bind to cis elements in the rice proliferating cell nuclear antigen gene. *The Plant Cell*, *9*(9), 1607–1619. https://doi.org/10.1105/tpc.9.9.1607

LaFountain, A. M., Chen, W., Sun, W., Chen, S., Frank, H. A., Ding, B., & Yuan, Y. (2017). Molecular Basis of Overdominance at a Flower Color Locus. *G3 Genes|Genomes|Genetics*, *7*(12), 3947–3954. https://doi.org/10.1534/g3.117.300336

Landis, J. B., Bell, C. D., Hernandez, M., Zenil-Ferguson, R., McCarthy, E. W., Soltis, D. E., & Soltis, P. S. (2018). Evolution of floral traits and impact of reproductive mode on diversification in the phlox family (Polemoniaceae). *Molecular Phylogenetics and Evolution*, *127*, 878–890. https://doi.org/10.1016/j.ympev.2018.06.035

Li, C., Potuschak, T., Colon-Carmona, A., Gutierrez, R. A., & Doerner, P. (2005). Arabidopsis TCP20 links regulation of growth and cell division control pathways. *Proceedings of the National Academy of Sciences*, *102*(36), 12978–12983. https://doi.org/10.1073/pnas.0504039102

Luo, D., Carpenter, R., Copsey, L., Vincent, C., Clark, J., & Coen, E. (1999). Control of Organ Asymmetry in Flowers of Antirrhinum. *Cell*, *99*(4), 367–376. https://doi.org/10.1016/S0092-8674(00)81523-8

Luo, D., Carpenter, R., Vincent, C., Copsey, L., & Coen, E. (1996). Origin of floral asymmetry in Antirrhinum. *Nature*, *383*(6603), 794–799. https://doi.org/10.1038/383794a0

Lynch, M., & Force, A. (2000). The Probability of Duplicate Gene Preservation by Subfunctionalization. *Genetics*, *154*(1), 459–473. https://doi.org/10.1093/genetics/154.1.459

Madrigal, Y., Alzate, J. F., González, F., & Pabón-Mora, N. (2019). Evolution of RADIALIS and DIVARICATA gene lineages in flowering plants with an expanded sampling in non-core eudicots. *American Journal of Botany*, *106*(3), 334–351. https://doi.org/10.1002/ajb2.1243

Maere, S., De Bodt, S., Raes, J., Casneuf, T., Van Montagu, M., Kuiper, M., & Van de Peer, Y. (2005). Modeling gene and genome duplications in eukaryotes. *Proceedings of the National Academy of Sciences*, *102*(15), 5454–5459. https://doi.org/10.1073/pnas.0501102102

Martin-Trillo, M., & Cubas, P. (2009). TCP genes: A family snapshot ten years later. *Cell Press*, *15*(1), 31–39.

Mondragón-Palomino, M., & Theißen, G. (2009). Why are orchid flowers so diverse? Reduction of evolutionary constraints by paralogues of class B floral homeotic genes. *Annals of Botany*, *104*(3), 583–594. https://doi.org/10.1093/aob/mcn258

Neal, P. R., Dafni, A., & Giurfa, M. (1998). Floral symmetry and its role in plant-pollinator systems: Terminology, Distribution, and Hypotheses. *Annual Review of Ecology and Systematics*, *29*(1), 345–373. https://doi.org/10.1146/annurev.ecolsys.29.1.345

Panchy, N., Lehti-Shiu, M., & Shiu, S.-H. (2016). Evolution of Gene Duplication in Plants. *Plant Physiology*, *171*(4), 2294–2316. https://doi.org/10.1104/pp.16.00523

Pang, H.-B., Sun, Q.-W., He, S.-Z., & Wang, Y.-Z. (2010). Expression pattern of CYC-like genes relating to a dorsalized actinomorphic flower in Tengia (Gesneriaceae). *Journal of Systematics and Evolution*, *48*(5), 309–317. https://doi.org/10.1111/j.1759-6831.2010.00091.x

Peirson, S. N., Butler, J. N., & Foster, R. G. (2003). Experimental validation of novel and conventional approaches to quantitative real-time PCR data analysis. *Nucleic Acids Research*, *31*(14), e73. https://doi.org/10.1093/nar/gng073

Preston, J. C., Barnett, L., Kost, M., Oborny, N., & Hileman, L. C. (2014). Optimization of virus-induced gene silencing to facilitate evo-devo studies in the emerging model species

Mimulus guttatus (Phrymaceae). *Annuals of the Missouri Botanical Garden*, *99*, 301–312.

Preston, J. C., & Hileman, L. C. (2009). Developmental genetics of floral symmetry evolution. *Trends in Plant Science*, *14*(3), 147–154. https://doi.org/10.1016/j.tplants.2008.12.005

Preston, J. C., & Hileman, L. C. (2012). Parallel evolution of TCP and B-class genes in Commelinaceae flower bilateral symmetry. *EvoDevo*, *3*(1), 6. https://doi.org/10.1186/2041-9139-3-6

Preston, J. C., Martinez, C. C., & Hileman, L. C. (2011). Gradual disintegration of the floral symmetry gene network is implicated in the evolution of a wind-pollination syndrome. *Proceedings of the National Academy of Sciences*, *108*(6), 2343–2348. https://doi.org/10.1073/pnas.1011361108

Raimundo, J., Sobral, R., Bailey, P., Azevedo, H., Galego, L., Almeida, J., Coen, E., & Costa, M. M. R. (2013). A subcellular tug of war involving three MYB-like proteins underlies a molecular antagonism in Antirrhinum flower asymmetry. *The Plant Journal*, *75*(4), 527–538. https://doi.org/10.1111/tpj.12225

Ree, R. H., & Donoghue, M. J. (1999). Inferring Rates of Change in Flower Symmetry in Asterid Angiosperms. *Systematic Biology*, *48*(3), 633–641.

Reeves, P., & Olmstead, R. (2003). Evolution of the TCP gene family in Asteridae: Cladistic and network approaches to understanding regulatory gene family diversification and its impact on morphological evolution. *Molecular Biology and Evolution*, *20*(12), 1997–2009. https://doi.org/10.1093/molbev/msg211

Rensing, S. A. (2014). Gene duplication as a driver of plant morphogenetic evolution. *Current Opinion in Plant Biology*, *17*, 43–48. https://doi.org/10.1016/j.pbi.2013.11.002

Reyes, E., Sauquet, H., & Nadot, S. (2016). Perianth symmetry changed at least 199 times in angiosperm evolution. *Taxon, 65*(5), 945–964. https://doi.org/10.12705/655.1

Rodriguez, I., Gumbert, A., Hempel de Ibarra, N., Kunze, J., & Giurfa, M. (2004). Symmetry is in the eye of the "beeholder": Innate preference for bilateral symmetry in flower-naive bumblebees. *Naturwissenschaften, 91*(8). https://doi.org/10.1007/s00114-004-0537-5

Sagawa, J. M., Stanley, L. E., LaFountain, A. M., Frank, H. A., Liu, C., & Yuan, Y. (2016). An R2R3- MYB transcription factor regulates carotenoid pigmentation in *Mimulus lewisii* flowers. *New Phytologist, 209*(3), 1049–1057. https://doi.org/10.1111/nph.13647

Sargent, R. D. (2004). Floral symmetry affects speciation rates in angiosperms. *Proceedings of the Royal Society B: Biological Sciences, 271*(1539), 603–608.

Sauquet, H., von Balthazar, M., Magallón, S., Doyle, J. A., Endress, P. K., Bailes, E. J., Barroso de Morais, E., Bull-Hereñu, K., Carrive, L., Chartier, M., Chomicki, G., Coiro, M., Cornette, R., El Ottra, J. H. L., Epicoco, C., Foster, C. S. P., Jabbour, F., Haevermans, A., Haevermans, T., … Schönenberger, J. (2017). The ancestral flower of angiosperms and its early diversification. *Nature Communications, 8*(1), 16047. https://doi.org/10.1038/ncomms16047

Sengupta, A., & Hileman, L. C. (2018). Novel traits, flower symmetry, and transcriptional autoregulation: New hypotheses from bioinformatic and experimental data. *Frontiers in Plant Science, 9*, 1561. https://doi.org/10.3389/fpls.2018.01561

Spencer, V., & Kim, M. (2017). Re"CYC"ling molecular regulators in the evolution and development of flower symmetry. *Seminars in Cell & Developmental Biology, 79*, 16–26. https://doi.org/10.1016/j.semcdb.2017.08.052

Stamatakis, A. (2006). RAxML-VI-HPC: Maximum likelihood-based phylogenetic analyses with thousands of taxa and mixed models. *Bioinformatics, 22*(21), 2688–2690. https://doi.org/10.1093/bioinformatics/btl446

Stanton, K. A., Edger, P. P., Puzey, J. R., Kinser, T., Cheng, P., Vernon, D. M., Forsthoefel, N. R., & Cooley, A. M. (2017). A Whole-Transcriptome Approach to Evaluating Reference Genes for Quantitative Gene Expression Studies: A Case Study in *Mimulus*. *G3 Genes|Genomes|Genetics*, *7*(4), 1085–1095. https://doi.org/10.1534/g3.116.038075

Vamosi, J. C., & Vamosi, S. M. (2010). Key innovations within a geographical context in flowering plants: Towards resolving Darwin's abominable mystery: Ecological limits vs. key innovations. *Ecology Letters*, *13*(10), 1270–1279. https://doi.org/10.1111/j.1461-0248.2010.01521.x

van der Niet, T., & Johnson, S. D. (2012). Phylogenetic evidence for pollinator-driven diversification of angiosperms. *Trends in Ecology & Evolution*, *27*(6), 353–361. https://doi.org/10.1016/j.tree.2012.02.002

Wang, J., Wang, Y., & Luo, D. (2010). LjCYC genes constitute floral dorsoventral asymmetry in Lotus japonicus. *Journal of Integrative Plant Biology*, *52*(11), 959–970. https://doi.org/10.1111/j.1744-7909.2010.00926.x

Wang, Z., Luo, Y., Li, X., Wang, L., Xu, S., Yang, J., Weng, L., Sato, S., Tabata, S., Ambrose, M., Rameau, C., Feng, X., Hu, X., & Luo, D. (2008). Genetic control of floral zygomorphy in pea (Pisum sativum L.). *Proceedings of the National Academy of Sciences*, *105*(30), 10414–10419. https://doi.org/10.1073/pnas.0803291105

Wessinger, C. A., & Hileman, L. C. (2020). Parallelism in flower evolution and development. *Annual Review of Ecology, Evolution, and Systematics*, *51*(1), 387–408. https://doi.org/10.1146/annurev-ecolsys-011720-124511

Wessinger, C. A., Rausher, M. D., & Hileman, L. C. (2019). Adaptation to hummingbird pollination is associated with reduced diversification in Penstemon. *Evolution Letters*, *3*(5), 521–533. https://doi.org/10.1002/evl3.130

Xu, S., Luo, Y., Cai, Z., Cao, X., Hu, X., Yang, J., & Luo, D. (2013). Functional Diversity of CYCLOIDEA-like TCP Genes in the Control of Zygomorphic Flower Development in Lotus japonicus. *Journal of Integrative Plant Biology*, *55*(3), 221–231. https://doi.org/10.1111/j.1744-7909.2012.01169.x

Yuan, Y. (2018). Monkeyflowers (Mimulus): New model for plant developmental genetics and evo-devo. *New Phytologist*. https://doi.org/10.1111/nph.15560

Yuan, Y., Sagawa, J. M., Stillo, V. S. D., & Bradshaw, H. D. (2013). Bulk segregant analysis of an induced floral mutant identifies a MIXTA-like R2R3 MYB controlling nectar guide formation in Mimulus lewisii. *Genetics*, *194*, 523–528. https://doi.org/10.1534/genetics.113.151225/-/DC1.

Yuan, Y., Sagawa, J. M., Young, R. C., Christensen, B. J., & Bradshaw, H. D. (2013). Genetic Dissection of a Major Anthocyanin QTL Contributing to Pollinator-Mediated Reproductive Isolation Between Sister Species of *Mimulus*. *Genetics*, *194*(1), 255–263. https://doi.org/10.1534/genetics.112.146852

Zhang, W., Kramer, E. M., & Davis, C. C. (2010). Floral symmetry genes and the origin and maintenance of zygomorphy in a plant-pollinator mutualism. *Proceedings of the National Academy of Sciences*, *107*(14), 6388–6393. https://doi.org/10.1073/pnas.0910155107

Zhang, W., Kramer, E. M., & Davis, C. C. (2012). Similar Genetic Mechanisms Underlie the Parallel Evolution of Floral Phenotypes. *PLoS ONE*, *7*(4), e36033. https://doi.org/10.1371/journal.pone.0036033

Zhang, W., Steinmann, V., Nikolov, L., Kramer, E., & Davis, C. (2013). Divergent genetic mechanisms underlie reversals to radial floral symmetry from diverse zygomorphic flowered ancestors. *Frontiers in Plant Science*, *4*, 302. https://doi.org/10.3389/fpls.2013.00302

Zhao, Y., Pfannebecker, K., Dommes, A. B., Hidalgo, O., Becker, A., & Elomaa, P. (2018). Evolutionary diversification of CYC/TB1-like TCP homologs and their recruitment for the control of branching and floral morphology in Papaveraceae (basal eudicots). *New Phytologist*, *220*(1), 317–331. https://doi.org/10.1111/nph.15289

Zhao, Z., Hu, J., Chen, S., Luo, Z., Luo, D., Wen, J., Tu, T., & Zhang, D. (2019). Evolution of CYCLOIDEA-like genes in Fables: Insights into duplication patterns and the control of floral symmetry. *Molecular Phylogenetics and Evolution*, *132*, 81–89. https://doi.org/10.1016/j.ympev.2018.11.007

Zhong, J., & Kellogg, E. A. (2015a). Stepwise evolution of corolla symmetry in CYCLOIDEA2-like and RADIALIS-like gene expression patterns in Lamiales. *American Journal of Botany*, *102*(8), 1260–1267. https://doi.org/10.3732/ajb.1500191

Zhong, J., & Kellogg, E. A. (2015b). Duplication and expression of *CYC2* -like genes in the origin and maintenance of corolla zygomorphy in Lamiales. *New Phytologist*, *205*(2), 852–868. https://doi.org/10.1111/nph.13104

Zhong, J., Preston, J. C., Hileman, L. C., & Kellogg, E. A. (2017). Repeated and diverse losses of corolla bilateral symmetry in the Lamiaceae. *Annals of Botany*, *119*(7), 1211–1223. https://doi.org/10.1093/aob/mcx012

Zhou, X.-R., Wang, Y.-Z., Smith, J. F., & Chen, R. (2008). Altered expression patterns of TCP and MYB genes relating to the floral developmental transition from initial zygomorphy to actinomorphy in Bournea (Gesneriaceae). *New Phytologist*, *178*(3), 532–543. https://doi.org/10.1111/j.1469-8137.2008.02384.x

Appendix A: Supplementary figures and tables

A) *Mimulus lewisii CYC1*

```
1    ATGTTCAACA AGAACACATA CATGATTCCT CAGGGTTCTG CTCCCTCCAC TTCTGTTCTT

61   GATCTCAACG GCAATGAAAT TTTGCTCCAC CACCACAATG TGTTTTCTGG CCACTACTTA

121  GCCACTAACG CTCCACCTGT CGAAGCTGCT GCCGCATTGT TCAATCAAGA TATCGGAGAA

181  ACTTCAGGAA CCCTAAACAC GTGTCCAAGA ACTCCGAAAA GAGATCGACA CAGCAAAATC

241  GACACTGCTC AAGGACCAAG GGACAGAAGA GTCAGGCTCT CGATAGGCGT CGCTCGAAAA

301  TTCTTCGATC TCCAGGAAAT GCTCGGTTTT GACAAGCCGA GCAAAACACT CGATTGGCTC

361  CTCACAAAAT CGAAAACCGC CATTAAGGAC CTCGTCAACA CAACGAAGCA AAGCTCGACT

421  GGAGCTGTTG TTTCCTCTCC TACTCCTTCG GACGAATGCG AGGTAGAAAA TGACGACTAT

481  GCCCTCGAAA AAGGGCCGTT TCTCGGTGCC GATTCGAAAG GGAAATCGGT GATGACGAGT

541  GGTAATAGCA AATTGCAGTA TAAAGGAGGT GCGAAGGATT TGATCGCGAA GGAGTCCAGG

601  GTTAAGGCGA GGGCGAGGGC GAGAGAAAGA ACGAGAGAGA AAATGTGCAT CAAGCAGCTC

661  AGTGAAACAA GAAACACTAC TACAGGCTAT TATGATCTGA TCAACCCTTC AAATAATAAT

721  ATCCCAATTC AGTACATGAA TAATCAGCTC GAGTATTGCA GAATATCGGG ATCGAGTGGA

781  AAATTATCGG GAATAAATTA TGCGATGAAT TATCAAGAAT GTGGAGGTGG AGACCTAATT

841  AATCAAGAAC CAGTGGTGAT CAAGAGGAAG GTGAAGCATC ATCCATCACC AATCTTGGGA

901  TTCCAGCCGA ATCTTATCCT TTCGAGAGAT TTGGGATCGA ACTACGGTTA TAGTAATGCC

961  ACTGATGATC AGAATTGGGA TCATATTAGT AGCTTTAATT CGTCACAATC CAACATATCT

1021 GCCATTTTGG ATCAGCACAA GTTCAACAAT AGTTGTTCAA GGAAAACTAG GAAAAAGTAC

1081 TATTGCATTA TTGATGCTGT AATTGTATGT TCTGCTACCT TTGATCTTCA GCAATCTGAG

1141 ATTTCAAAGG TTGCATAA
```

B) *Mimulus lewisii CYC2*

```
1    ATGTTCAGCA CGAACAATTA CCTGCTTCCT CAGTACTTTT CATCATCATC ATCATCATCA

61   CCATCATCTC TATACCCTCG CCCAAATGCT TCTCTTGTTG ACCTAAACAG CGTCGAATTC

121  TTGTTCCACC ACCACCCGGA AATGTTCTCC GGCCACTATT TAGCTGCTGC CGCCAACGCT

181  CAGCCGTTCA TCCACGCTGC TGCTCTGCTC AATCAAGACG ACAGCAGAAC ACTAAACGGA

241  GAAGCCCCTT CTGCCACCAC AGTGGCGGCA AACTCGCTTC AAAGAAAGCA ACCCGTGAAA

301  AAGGACCGCC ACAGTAAGAT ATTCACTGCT CAAGGTCCGA GGGATCGAAG AGTACGGCTC
```

```
361  TCCATCGGCA TTGCTCGAAA GTTCTTCGAC CTTCAAGAAA TGCTAGGTTT CGACAAGCCA

421  AGCAAAACCC TCGATTGGCT GCTCACGAAG TCGAAAGCCG CCATTAAAGA GCTCGTGCAG

481  ATGAAAGAAA ACGCTAGTTG CGCTAATAAG AGCGCTTCTT CTCCCTCCGA ATGTGAGCTT

541  ATCTCTTCGG AATCGAACGG TGAGGCTTTT GAAATCGGGG CGGACACGAA GAAGAAATTT

601  GTTAAGGAAT CGAGGGCGAA GGCGAGAGCT AGGGCTAGGG AAAGAACAAA AGAGAAAATG

661  AGCATCAAGA ATAACATGGG TTCTGATGAT TTGAACCCTT TACCAGTCCC AATTCAATAT

721  AGAAATAATC AAGTTGACTT ATTCCAATCA TCAGCTGCAG GTGCTCAAGA CCCGAGTTCG

781  AACTACGGTG TCCTAATTCA AGAATCTATT GTGGTCAAAA GGAAGATGAA GAGCCCTTCG

841  TTTTTCGGGT TTCAGCAAAA CGTTTCTGTT TCGAGAGATT CGAGTTCGAA CTACGGTGTC

901  CCGTCTGCTA ATAATGCCGC TGAAAATTGG GATATTTGCA GCTTCACTTC TCAGTCCAAC

961  TTGTGTGCTA CTTTGGATCA GCACAAGTTC ATCAATAGGT AA
```

Figure A1. Coding sequence and RNAi target sequences for *MlCYC1* and *MlCYC2*. (A) *MlCYC1* coding sequence, 270 bp used to construct *MlCYC1* RNAi hairpin highlighted. (B) *MlCYC2* coding sequence, 180 bp used to construct *MlCYC2* RNAi hairpin highlighted.

Table A1. *M. lewisii* qRT-PCR primers (5' to 3').

Gene	Forward primer	Reverse primer
MlCYC1	AGGAGGTGCGAAGGATTTGATC	AGTAGTGTTTCTTGTTTCACTGAGCT
MlCYC2	TTTGAAATCGGGGCGGACAC	TTGGGACTGGTAAAGGGTTCAAA
MlRAD4	ACGGAGGAAGAAGTCAAACGG	TACTTACGATCGGCACCACTTTT
MlRAD5	GCAAAACCGCCGAAGAAGTC	CCATTAGTGGTAGTTGAGGTGGTCC
MlIFA	GAAGCCTATGACGCACCCAC	GCCCTCCTCCCACTCATCAT

Table A2. *M. lewisii* PCR primers with restriction sites (5' to 3').

Gene	Forward primer	Reverse primer
*MlCYC1*_424_RE	GTTCTAGACCATGGCGAGT ATTGCAGAATATCGGGA	GTGGATCCGGCGCGCCGGCAGA TATGTTGGATTGTAGTGACG
*MlCYC2*_2324_RE	GTTCTAGACCATGGTCCAA TCATCAGCTGCAGGT	GTGGATCCGGCGCGCCGCGGCA TTATTAGCAGACGG

Table A3. Vector specific PCR primers (5' to 3'). Primer pair pFGC5941_2372-F and pFGC5941_3082-R were used to amplify the left insert and primer pair pFGC5941_3930-F and pFGC5941_4430-R were used to amplify the right insert.

Primer ID	Primer	Target fragment
pFGC5941_2372-F	CTTCATCGAAAGGACAGTAGAA	Left arm T-DNA
pFGC5941_3082-R	CCAAACAGGCTCATAGATACT	Left arm T-DNA
pFGC5941_3930-F	TGTACATCAGAATGTTTCTGAC	Right arm T-DNA
pFGC5941_4430-R	CGCTCTATCATAGATGTCGCTA	Right arm T-DNA

Table A4. *M. lewisii* insert and vector specific PCR primers (5' to 3') for screening double RNAi lines. Primer pair *MlCYC1*_424-R and pFGC5941_2372-F were used to amplify the *MlCYC1* insert and primer pair *MlCYC2*_2324-R and pFGC5941_4430-R were used to amplify the *MlCYC2* insert.

Primer ID	Primer	Target fragment
*MlCYC1*_424-R	GGCAGATATGTTGGATTGTGACG	*MlCYC1*
pFGC5941_2372-F	CTTCATCGAAAGGACAGTAGAA	*MlCYC1*
*MlCYC2*_2324-R	GCGGCATTATTAGCAGACGG	*MlCYC2*
pFGC5941_4430-R	CGCTCTATCATAGATGTCGCTA	*MlCYC2*

Table A5. Accession numbers for ECE-*CYC2* genes used in ortholog analysis.

Species	Gene	NCBI Accession #
Antirrhinum majus	*AmCYC, AmDICH*	Y16313, AF199465
Mimulus guttatus	*MgCYC2A, MgCYC2B*	H00528, K00858
Mimulus ringens	*MrCYC2A, MrCYC2B*	KM526894, KM526920
Phryma leptostachya	*PlCYC2A, PlCYC2B*	KM526895, KM526921

Table A6. Table of floral trait measurements for *M. lewisii* LF10 and RNAi lines.

Line	*n*	Nectar guide ridge count			Dorsal petal width:length			Lateral petal width:length			Ventral petal width:length		
		Mean ± SD	Range	*P*-value	Mean ± SD	Range	*P*-value	Mean ± SD	Range	*P*-value	Mean ± SD	Range	*P*-value
LF10	23; 5	2 ± 0.0	2		1.163 ± 0.07253	1.051-1.289		0.7440 ± 0.0891	0.509-0.874		0.8525 ± 0.08051	0.7102-1.015	
***MICYC1_RNAi* (combined)**	20; 4	4 ± 0.0	4	5.976E-12	1.090 ± 0.06378	0.933-1.24	0.001146	0.8272 ± 0.05789	0.738-0.93	0.0009398	0.8707 ± 0.07486	0.7540-1.010	0.4492
MICYC1_RNAi-13	5	4 ± 0.0	4	5.976E-12	1.083 ± 0.02144	1.721-1.836	0.02379	0.8752 ± 0.5097	0.8075-0.9300	0.004072	0.8406 ± 0.1117	0.7876-0.8689	0.7513
MICYC1_RNAi-14	5	4 ± 0.0	4	5.976E-12	1.055 ± 0.08406	0.933-1.137	0.006737	0.8729 ± 0.02103	0.8391-0.8936	0.003883	0.8290 ± 0.06443	0.7809-0.9423	0.5486
MICYC1_RNAi-15	5	4 ± 0.0	4	5.976E-12	1.132 ± 0.06752	1.070-1.240	0.3862	0.7663 ± 0.02065	0.7376-0.7873	0.5891	0.8839 ± 0.1011	0.7544-1.010	0.4562
MICYC1_RNAi-16	5	4 ± 0.0	4	5.976E-12	1.089 ± 0.05864	1.023-1.164	0.04371	0.7941 ± 0.03042	0.7652-0.8303	0.2313	0.9288 ± 0.05899	0.8635-1.007	0.05700
***MICYC2_RNAi* (combined)**	28; 6	2.339 ± 0.3862	2-3	0.0001102	1.186 ± 0.1693	0.896-1.63	0.5604	0.7837 ± 0.07067	0.684-0.93	0.08229	0.8693 ± 0.06079	0.7460-1.005	0.3988
MICYC2_RNAi-1	5	2.200 ± 0.2734	2-2.5	0.1778	1.154 ± 0.05163	1.094-1.221	0.7960	0.8364 ± 0.08223	0.7303-0.9302	0.04324	0.8637 ± 0.08432	0.7903-1.005	0.7821
MICYC2_RNAi-3	5	2.300 ± 0.2449	2-2.5	0.07048	1.449 ± 0.1504	1.180-1.630	1.620E-06	0.7723 ± 0.04645	0.7035-0.8426	0.5035	0.9054 ± 0.06014	0.8472-0.9785	0.02871
MICYC2_RNAi-4	5	2.500 ± 0.5000	2-3	0.08901	1.020 ± 0.09327	0.8959-1.151	0.0007820	0.7206 ± 0.02058	0.6845-0.7336	0.5702	0.8353 ± 0.05699	0.7459-0.9030	0.6551
MICYC2_RNAi-5	4	2.800 ± 0.4472	2-3	0.01613	1.117 ± 0.05569	1.057-1.191	0.2395	0.7397 ± 0.05335	0.6847-0.7999	0.9259	0.8933 ± 0.05127	0.8307-0.9482	0.3415
MICYC2_RNAi-8	5	2.200 ± 0.2739	2-2.5	0.1778	1.180 ± 0.1348	0.9887-1.355	0.6951	0.7808 ± 0.05919	0.7073-0.8428	0.3895	0.8773 ± 0.05311	0.8040-0.9271	0.5197
MICYC2_RNAi-11	4	2.125 ± 0.2500	2-2.5	0.3910	1.178 ± 0.09469	1.052-1.273	0.7292	0.8582 ± 0.05220	0.8010-0.9198	0.02092	0.8394 ± 0.02846	0.7994-0.8646	0.7540
MICYC1_RNAi-13:MICYC2_RNAi-3	17; 3	4.500 ± 4.324	4-5	8.448E-26	0.9973 ± 0.09501	0.8318-1.133	2.450E-07	0.8596 ± 0.05467	0.7531-0.9671	3.137E-05	0.8275 ± 0.1094	0.7234-1.150	0.4102
MICYC1_RNAi-13:MICYC2_RNAi-8	22; 4	4.295 ± 0.3671	4-5	1.804E-30	1.007 ± 0.06429	0.8815-1.129	1.501E-09	0.9281 ± 0.1087	1.116-1.578	7.399E-10	0.8123 ± 0.09523	0.6743-0.9936	0.1329
MICYC1_RNAi-13:MICYC2_RNAi-5	25; 5	4.840 ± 0.3452	4-5	4.196E-37	0.9863 ± 0.08904	0.8261-1.161	1.606E-09	0.8725 ± 0.06112	0.7913-1.060	4.593E-07	0.8402 ± 0.05141	0.7669-0.9267	0.5270
MICYC2_RNAi-5:MICYC1_RNAi-13	28; 5	4.831 ± 0.3392	4-5	5.556E-39	0.9450 ± 0.07249	0.8123-1.095	2.112E-14	0.9006 ± 0.06296	0.8039-1.002	1.985E-09	0.8344 ± 0.0545	0.7433-0.9375	0.3457

Dorsal-dorsal petal angle (Deg)			Dorsal-lateral petal angle (Deg)			Ventral-lateral petal angle (Deg)			Dorsal corolla tube flare (Deg)			Ventral corolla tube flare (Deg)		
Mean ± SD	Range	*P*-value	Mean ± SD	Range	*P*-value	Mean ± SD	Range	*P*-value	Mean ± SD	Range	*P*-value	Mean ± SD	Range	*P*-value
3.881 ± 6.517	0-18.89		86.95 ± 10.11	70.59-105.2		10.12 ± 4.419	0-22.21		119.5 ± 8.140	107.2-138.9		136.9 ± 7.056	125.2-150.2	
16.93 ± 21.66	0-61.53	0.008748	63.10 ± 8.842	40.35-74.31	3.783E-10	15.39 ± 8.206	0-30.51	0.01088	122.2 ± 4.794	114.9-130.6	0.2101	143.7 ± 6.428	131.6-158.6	0.002568
23.51 ± 18.64	0-51.87	0.0002710	61.48 ± 1.821	58.81-63.83	8.210E-06	24.78 ± 6.711	13.57-30.51	1.750E-06	116.5 ± 0.9576	114.9-117.5	0.7156	145.0 ± 5.070	139.5-151.1	0.08215
22.92 ± 31.53	0-61.525	0.009332	52.52 ± 10.60	40.35-63.54	2.840E-07	14.91 ± 5.769	10.81-23.79	0.04719	122.5 ± 4.696	116.1-123.4	0.3075	142.0 ± 6.268	131.6-147.4	0.3266
15.86 ± 21.77	0-41.80	0.02805	68.77 ± 3.130	66.64-74.31	5.620E-04	12.87 ± 7.890	0-19.03	0.2851	124.4 ± 4.184	119.6-130.6	0.1478	149.0 ± 6.339	142.7-158.6	0.009132
5.416 ± 12.11	0-27.08	0.6875	69.61 ± 3.079	66.60-73.96	8.970E-04	9.000 ± 3.139	5.318-13.15	0.5966	125.4 ± 2.940	122.2-129.2	0.09179	138.9 ± 4.715	132.4-143.8	0.8498
13.09 ± 20.16	0-65.97	0.04100	67.00 ± 7.743	53.82-77.62	2.027E-10	13.63 ± 6.903	0-26.29	0.04041	131.8 ± 7.314	114.7-146.9	1.730E-10	143.0 ± 4.901	133.4-152.4	0.000958
5.797 ± 12.96	0-28.99	0.6255	67.72 ± 7.345	56.83-76.17	4.622E-04	17.04 ± 4.137	12.85-22.30	0.003586	130.0 ± 9.394	114.7-138.3	0.01459	139.5 ± 4.491	133.4-144.9	0.7309
0.0 ± 0.0	0	0.2009	63.79 ± 7.557	53.82-73.89	6.384E-05	11.31 ± 4.968	5.598-18.37	0.6054	141.1 ± 3.704	136.9-146.9	1.140E-05	150.2 ± 2.308	145.9-152.4	0.003026
49.25 ± 10.93	35.66-65.97	1.760E-12	69.90 ± 5.793	62.07-76.40	1.276E-03	14.34 ± 6.516	7.894-18.66	0.08715	131.3 ± 5.844	124.5-136.6	0.005096	140.1 ± 1.623	138.8-142.8	0.6114
9.619 ± 12.76	0-26.92	0.1726	62.40 ± 7.447	56.93-73.33	1.015E-04	3.631 ± 3.152	0-7.695	0.009806	124.3 ± 3.880	120.3-128.7	0.1984	143.3 ± 2.975	140.5-147.5	0.2207
0.0 ± 0.0	0	0.2009	73.52 ± 3.797	67.78-77.62	7.635E-03	14.00 ± 4.171	8.25-18.52	0.08483	131.8 ± 4.490	128.0-139.2	0.003334	144.3 ± 3.755	139.4-149.0	0.1113
13.20 ± 16.06	0-32.60	0.0478	62.94 ± 9.998	54.74-77.21	1.804E-04	20.92 ± 6.447	11.55-26.29	0.000272	133.2 ± 5.509	126.6-141.1	0.001662	139.9 ± 2.676	136.2-143.2	0.6416
68.10 ± 9.599	47.65-83.28	2.467E-25	46.73 ± 8.185	30.63-59.16	4.937E-16	27.41 ± 8.943	17.71-55.88	9.509E-10	134.0 ± 4.580	125.5-142.1	9.833E-08	141.8 ± 3.471	134.1-149.1	0.09326
73.03 ± 13.09	57.52-109.7	1.793E-25	44.09 ± 9.280	17.14-59.63	1.759E-18	25.28 ± 9.783	7.972-40.54	2.999E-08	134.3 ± 4.447	127.1-143.7	2.717E-09	140.7 ± 3.006	135.3-145.7	0.1729
63.72 ± 19.41	0-81.59	2.864E-18	49.94 ± 7.150	30.13-64.56	4.795E-19	24.53 ± 8.214	9.918-40.84	1.795E-09	137.1 ± 4.547	129.3-147.5	1.035E-11	142.1 ± 3.521	133.2-148.5	0.0341
72.50 ± 7.428	60.26-90.09	3.894E-36	48.58 ± 6.371	37.25-62.22	1.183E-21	27.73 ± 9.365	0-39.60	7.111E-11	137.8 ± 2.955	132.1-143.9	1.940E-14	143.2 ± 2.037	138.1-146.5	0.002643